HHS Public Access

Author manuscript

Nat Neurosci. Author manuscript; available in PMC 2023 October 01.

Published in final edited form as:

Nat Neurosci. 2023 April ; 26(4): 638–649. doi:10.1038/s41593-023-01282-y.

Intrinsic activity development unfolds along a sensorimotor–association cortical axis in youth

Valerie J. Sydnor[1,2], **Bart Larsen**[1,2], **Jakob Seidlitz**[2,3,4], **Azeez Adebimpe**[1,2], **Aaron F. Alexander-Bloch**[2,3,4], **Dani S. Bassett**[2,5,6,7,8,9], **Maxwell A. Bertolero**[1,2], **Matthew Cieslak**[1,2], **Sydney Covitz**[1,2], **Yong Fan**[10], **Raquel E. Gur**[2,3,4], **Ruben C. Gur**[2,4], **Allyson P. Mackey**[11], **Tyler M. Moore**[2], **David R. Roalf**[2], **Russell T. Shinohara**[12,13,14], **Theodore D. Satterthwaite**[1,2,4,12,14,*]

[1.] Penn Lifespan Informatics and Neuroimaging Center (PennLINC), Perelman School of Medicine, University of Pennsylvania, Philadelphia, PA, 19104, USA

[2.] Department of Psychiatry, Perelman School of Medicine, University of Pennsylvania, Philadelphia, PA, 19104, USA

[3.] Department of Child and Adolescent Psychiatry and Behavioral Science, The Children's Hospital of Philadelphia, Philadelphia, PA, 19104, USA

[4.] Penn-CHOP Lifespan Brain Institute, Perelman School of Medicine, Children's Hospital of Philadelphia, Philadelphia, PA, 19104, USA

[5.] Department of Bioengineering, School of Engineering and Applied Science, University of Pennsylvania, Philadelphia, PA, 19104, USA

[6.] Department of Electrical and Systems Engineering, School of Engineering and Applied Science, University of Pennsylvania, Philadelphia, PA, 19104, USA

[7.] Department of Physics and Astronomy, College of Arts and Sciences, University of Pennsylvania, Philadelphia, PA, 19104, USA

[*]Correspondence: Theodore D. Satterthwaite, sattertt@pennmedicine.upenn.edu.

AUTHOR CONTRIBUTIONS STATEMENT

VJS conceived of the neurodevelopmental framework and designed the study with BL and TDS. REG, RCG, and TDS provided resources and supervised collection of the neuroimaging data. DRR and TDS curated and quality checked the neuroimaging data. VJS, AA, MAB, MC, and SC processed the neuroimaging data with software tools developed by AA, MC, and SC. VJS implemented all statistical analyses with R code written by VJS and BL. AAB and RTS provided input on statistical approaches. DSB and YF provided input on image analytic approaches. BL conducted an internal code review and technical replication of all study findings. JS provided data used to derive the sensorimotor-association axis. TMM generated the neighborhood environment factor scores and APM provided expert guidance on environmental analyses. VJS generated all figures. VJS wrote the original draft and all authors (VJS, BL, JS, AA, AAB, DSB, MAB, MC, SC, YF, REG, RCG, APM, TMM, DRR, RTS, TDS) reviewed and revised the final draft.

COMPETING INTERESTS STATEMENT

The authors declare the following competing interest: RTS receives consulting income from Octave Bioscience for work wholly unrelated to the present research. All other authors declare no competing interests.

CODE AVAILABILITY

Neuroimaging data were processed with containerized software packages available on dockerhub. Resting-state functional MRI data were processed with fMRIPrep 20.2.3 (https://hub.docker.com/r/nipreps/fmriprep/tags) and xcp_d 0.0.4 (https://hub.docker.com/r/pennlinc/xcp_abcd/tags). Following image processing, all subsequent analyses and statistics were conducted in R 4.0.2 (https://www.r-project.org) using original analysis code and Connectome Workbench 1.5.0 tools (https://www.humanconnectome.org/software/get-connectome-workbench). Original code, including code used to calculate fluctuation amplitude, fit regional GAMs, contextualize developmental and environmental effects, and perform sensitivity analyses, has been deposited at Zenodo and is available at https://doi.org/10.5281/zenodo.7606653. A detailed description of the code and guide to code implementation is additionally provided at https://pennlinc.github.io/spatiotemp_dev_plasticity/.

[8.] Department of Neurology, Perelman School of Medicine, University of Pennsylvania, Philadelphia, PA, 19104, USA

[9.] Santa Fe Institute, Santa Fe, NM, 87501, USA

[10.] Department of Radiology, Perelman School of Medicine, University of Pennsylvania, Philadelphia, PA, 19104, USA

[11.] Department of Psychology, University of Pennsylvania, Philadelphia, PA, 19104, USA

[12.] Penn Statistics in Imaging and Visualization Endeavor (PennSIVE), Perelman School of Medicine, University of Pennsylvania, Philadelphia, PA, 19104, USA

[13.] Department of Biostatistics, Epidemiology and Informatics, Perelman School of Medicine, University of Pennsylvania, Philadelphia, PA, 19104, USA

[14.] Center for Biomedical Image Computing and Analytics, University of Pennsylvania, Philadelphia, PA, 19104, USA.

Abstract

Animal studies of neurodevelopment have shown that recordings of intrinsic cortical activity evolve from synchronized and high amplitude to sparse and low amplitude as plasticity declines and the cortex matures. Leveraging resting-state functional MRI (fMRI) data from 1,033 youth (8–23 years), we find that this stereotyped refinement of intrinsic activity occurs during human development and provides evidence for a cortical gradient of neurodevelopmental change. Declines in the amplitude of intrinsic fMRI activity were initiated heterochronously and coupled to the maturation of intracortical myelin, a developmental plasticity regulator. Spatiotemporal variability in developmental trajectories was organized along a hierarchical, sensorimotor-association cortical axis from ages 8–18. The sensorimotor-association axis furthermore captured variation in associations between youths' neighborhood environments and intrinsic fMRI activity: findings suggest that the effects of environmental disadvantage on the maturing brain diverge most across this axis during mid-adolescence. These results uncover a hierarchical neurodevelopmental axis and offer insight into the progression of cortical plasticity in humans.

Keywords

Neurodevelopment; spontaneous activity; sensorimotor-association axis; hierarchy; plasticity; myelin; functional MRI; BOLD fluctuations; neighborhood environment; socioeconomic circumstances

INTRODUCTION

Elucidating how developmental plasticity spatially and temporally progresses across the human cortex has implications for understanding healthy brain development as well as windows of developmental vulnerability and opportunity[1–3]. In particular, demarcating regionally-specific periods of enhanced and diminished malleability can provide insight into which cortical regions will be maximally impacted by insults and interventions at distinct developments stages. Prior studies have therefore aimed to uncover the spatiotemporal

evolution of neurodevelopmental change across the cortical mantle. Such studies have consistently shown that postnatal neurodevelopment is heterochronous, with sensory and motor cortices maturating earlier than association cortices[4]; this temporal trend has been shown for cortical volume[5,6], connectivity[7], myelination[8,9], and cellular properties[10,11]. However, beyond this coarse division there is marked spatiotemporal developmental variability that remains under-characterized. We recently proposed a unifying framework that contextualizes asynchronous maturation between sensorimotor and association cortices as two ends of a continuous axis of neurodevelopmental plasticity[4]. This framework posits that during childhood and adolescence, developmental plasticity progresses along the sensorimotor-association (S-A) cortical axis: a dominant, hierarchical axis of human brain organization along which diverse neurobiological properties are patterned[4,12–15].

In the present study, we aimed to empirically evaluate our hypothesis that plasticity unfolds along the S-A axis by studying the developmental refinement of intrinsic (i.e., spontaneous or non-evoked) activity: a putative functional marker of local plasticity described in animal models. Studies of the developing murine sensory cortex have provided evidence that a potentiation of high amplitude, synchronized intrinsic activity characterizes earlier stages of development with heightened plasticity[16–18]. As plasticity declines and the cortex matures, intrinsic activity evolves from prevalent and globally synchronized to suppressed and sparse, becoming more heterogeneously distributed in space and time in adult cortex[18–21]. This stereotyped refinement of intrinsic activity has been linked to maturational increases in inhibitory neurotransmission and intracortical myelination—two plasticity-regulating processes that refine cortical circuit dynamics[17,22–25]. Accordingly, this stereotyped refinement of intrinsic activity provides an ongoing readout of local circuit plasticity, with more correlated, high amplitude spontaneous neural recordings serving as a functional hallmark of still-malleable cortices[16,17,26,27]. Importantly, intrinsic cortical activity can be studied non-invasively with resting-state functional MRI (fMRI), which provides an opportunity to characterize the spatiotemporal maturation of a potential plasticity signature in the human brain.

Simultaneous fMRI and electrophysiology or calcium recordings have demonstrated how low frequency fluctuations in the resting fMRI blood oxygen level dependent (BOLD) signal are coupled with changes in intrinsic neural activity patterns[28–31]. A greater level of intrinsic activity and more synchronized activity—activity characteristic of immature, plastic cortices—increases the amplitude of low frequency BOLD fluctuations. It has therefore been hypothesized that the amplitude of low frequency fluctuations[32], or BOLD “fluctuation amplitude”, will be higher when cortical plasticity is enhanced[26,33]. Indeed, experimentally manipulating biological regulators of developmental plasticity has been shown to elicit changes in local BOLD fluctuations[34]. Moreover, in a recent landmark study of human brain plasticity, deprivation-induced somatomotor cortex plasticity produced local increases in BOLD fluctuation amplitude[35].

Here we harness BOLD fluctuation amplitude to index spatially-localized, age-dependent changes in intrinsic activity and test the overarching framework that developmental programs cascade hierarchically along the cortex’s S-A axis in youth. We expected that the development of fluctuation amplitude would be primarily characterized by

heterochronous declines along the S-A axis. Moreover, we predicted that declines in fluctuation amplitude would be influenced by the maturation of intracortical myelin, which constrains plasticity in developing neural circuits and refines spontaneous firing[25]. Last, we hypothesized that youths' developmental environments would impact the maturation of this measure. Instrumental work in animal models has shown that enriched (versus deprived) developmental environments affect the maturation of plasticity-regulating mechanisms, including intracortical myelin[36], inhibitory interneurons[37], and perineural nets[38], typically in a manner that facilitates continued plasticity[39]. Data from human studies have additionally shown that youth raised in more socioeconomically disadvantaged environments exhibit characteristics that could reflect a faster pace of biological and brain development (e.g., faster cortical thinning)[39–41]. Cross-species findings thus indicate that environmental deprivation may accelerate cortical development by prematurely limiting plasticity. We explore this possibility by studying whether greater environmental disadvantage is associated with functional markers suggestive of lower cortical plasticity during youth. As described below, our in vivo analysis of a signature of neurodevelopmental plasticity illuminated by animal models reveals that the S-A axis captures not only the hierarchical layout of diverse cortical properties, but also the temporal patterning of developmental change and effects of the developmental environment.

RESULTS

We studied how intrinsic activity is refined across the developing cortex in a cross-sectional sample of 1,033 youth ages 8–23 years old. Fluctuation amplitude, computed as the average power of low frequency (0.01–0.08 Hz) fluctuations in the time-varying fMRI signal, was used to index the overall level and coherence of intrinsic cortical activity. Greater and more synchronized neural activity increases the power of neural recordings and has been shown to increase the amplitude of BOLD fluctuations[29–31]. To characterize maturational changes in BOLD fluctuation amplitude in individual cortical regions, we fit region-specific generalized additive models (GAMs) with a smooth term for age; sex and in-scanner head motion were included as linear covariates. Each GAM estimates a smooth function (the model age fit) that describes the relationship between fluctuation amplitude and age, thereby modeling a region's developmental trajectory. The first derivative of this smooth function represents the rate of change in fluctuation amplitude at a given developmental timepoint. We tested whether GAM-derived developmental effects provide support for a hierarchical neurodevelopmental framework. We also confirmed that effects were robust to controls for in-scanner motion, medication use, vascular effects, T2* signal strength, global BOLD properties, and cortical atlas.

Development of intrinsic fMRI activity varies across the cortex

Fluctuation amplitude significantly changed with age in the developmental window studied in nearly all cortical regions ($p_{FDR} < 0.05$ in 95% of regions). To provide insight into the overall magnitude and direction of regional age effects, we calculated the variance explained by age (partial R^2; i.e., the effect magnitude) and the sign of the average derivative of the age fit (i.e., the effect direction). The magnitude and direction of age effects differed across the cortex (Fig. 1a), signifying that there is variability in the maturation of

intrinsic activity across the developing cortex. Indeed, by visualizing age fits across regions we observed a cortical continuum of developmental trajectories ranging from large and prolonged decreases (light yellow fits in Fig. 1b) to inverted U-shaped curves (dark purple fits). Nearly all sensory regions showed continuous declines in fluctuation amplitude from early childhood through adolescence, as illustrated by the model fit for area V1 (Fig. 1c, top panel) which significantly decreased until age 18 years. This age fit is consistent with a progressive reduction, sparsification, or decorrelation of non-evoked cortical activity with age. In contrast, in select cortical regions such as the midcingulate gyrus (Fig. 1c, middle panel), fluctuation amplitude only began to decline in later childhood or early adolescence. Finally, many regions in transmodal association cortex (e.g., the dorsolateral prefrontal cortex; Fig. 1c, bottom panel) displayed significant increases in fluctuation amplitude until early to mid-adolescence, typically followed by amplitude decreases. This inverted U-shaped trajectory suggests there is heightened, synchronized activity in transmodal cortices at the start of adolescence.

We examined whether regional age fits differed by sex or could be accounted for by differences in participant pubertal stage. We first tested for age-by-sex interactions in each cortical region and found no significant effects ($p_{FDR} > 0.05$ for all interactions), indicating that the timing of developmental change did not significantly differ between males and females in this age range. Next, we explored the potential impact of puberty by including participant pubertal stage (pre-pubertal, mid-pubertal, or post-pubertal) as a factor in regional GAMs. While the linear effects of pubertal stage on fluctuation amplitude tended to cohere with the observed age effects (positive effects in frontal transmodal regions, negative effects in posterior unimodal regions), pubertal stage did not explain significant variance in fluctuation amplitude above and beyond age in any cortical region ($p_{FDR} > 0.05$ for all pubertal stage effects). Moreover, accounting for pubertal stage did not alter regional age fits or age effects; age effects were highly correlated when age was modeled alone and when both age and pubertal stage were modeled together ($r = 0.89$). These findings suggest that age-dependent changes in intrinsic fMRI activity are heterogeneous across the cortex, present across sexes, and not driven by pubertal stage. More broadly, the present results establish that maturational trajectories diverge between sensory and association cortices.

Development of intrinsic fMRI activity mirrors myelin maturation

Prior work in animal models has shown that as the cortex transitions from plastic to mature, intrinsic cortical activity develops from prevalent and synchronized—producing high amplitude neural recordings—to sparse and decorrelated—producing lower amplitude recordings. These observations suggest that age-dependent changes in the amplitude of BOLD fluctuations could, in part, reflect changes in cortical plasticity[26,35]. We therefore endeavored to understand whether the development of fluctuation amplitude is related to the maturation of intracortical myelination: a key regulator and restrictor of cortical plasticity. We leveraged the recent work of Baum et al. (2022)[42] who studied the development of the T1w/T2w ratio, a structural MRI measure sensitive to cortical myelin content, in a large, independent sample of youth ages 8–21 years old. These authors quantified the magnitude of age-related myelination (the partial R^2 of the T1w/T2w ratio age effect) and demarcated the age of maximal myelin growth (the age with a maximal rate of

T1w/T2w ratio increase) within individual cortical regions. In comparing T1w/T2w ratio and fluctuation amplitude neurodevelopmental features, we unveiled substantial spatial and temporal correspondence between the refinement of these measures with age. Age-related changes (indexed by the signed partial R^2) in these two putative plasticity-sensitive measures were strongly inversely correlated across cortical regions ($r = -0.67$, $p_{spin} = 0.00045$), with regions showing larger increases in myelin content from childhood to early adulthood also showing larger decreases in BOLD signal amplitude (Fig. 2a–b). This finding accords with ample evidence of causal, bidirectional relationships between changes in neural activity patterns and changes in myelination[43,44] and suggests a possible mechanistic link between microstructural refinement and changes in circuit activity during brain development.

To further study this link, we investigated whether there was a temporal relationship between increases in the T1w/T2w ratio and decreases in fluctuation amplitude. We first quantified the age at which fluctuation amplitude began to significantly decrease in each region and found that initial decreases in fluctuation amplitude were staggered heterochronously across the cortex, with select medial prefrontal and frontopolar regions showing no period of significant decline. Nearly half of regions (46%) showed a significant decrease in fluctuation amplitude at age 8, implying that BOLD amplitude in these regions likely begins to decline prior to the youngest age studied in this dataset. Across the rest of the cortex, however, fluctuation amplitude began to decline later in youth; in these cortices, a greater delay in the onset of fluctuation amplitude decline was associated with a later peak in the rate of T1w/T2w-indexed cortical myelination ($r = 0.64$, $p_{spin} = 0.01565$; Fig. 2c–d). Notably, ages of fluctuation amplitude decrease onset and maximal T1w/T2w increase were not simply correlated but also showed a minimal temporal offset in years, indicating that they were closely coupled in time (average offset = 0.7 years; see also the best fit line for Fig. 2d). Taken together, these results appear to link later-onset reductions in the amplitude of spontaneous fMRI activity to delayed maturation of a main regulator of developmental plasticity.

Developmental variability is patterned along the S-A axis

A primary goal of this work was to systematically assess whether the sequence of neurodevelopmental change progresses hierarchically across the cortical mantle. Having observed that fluctuation amplitude development tightly paralleled development of a plasticity regulator and broadly diverged between sensorimotor and association cortices, we next sought to determine whether developmental patterns spatially conformed to the S-A axis[4]. The S-A axis is a prominent axis of cortical variation that is rank ordered from primary sensory and motor cortices (lowest ranks) to modality-selective and multimodal cortices, then progressing to transmodal heteromodal and paralimbic cortices (highest ranks). This axis captures the concerted patterning of heterogeneous structural, metabolic, cellular, molecular, transcriptomic, and electrophysiological properties across the cortex[4,12–15,45]. Moreover, the S-A axis is spatially coupled to the brain's anatomical[45], functional[14], and evolutionary[46] hierarchies, thus each cortical region's rank in the axis reflects its relative position in a global cortical hierarchy.

We first examined whether inter-regional differences in the development of fluctuation amplitude reflected inter-regional differences in S-A axis rank. Region-wise age effects and S-A axis ranks were correlated ($r = 0.54$, $p_{spin} = 0.00215$), with large negative age effects characterizing the S-A axis's sensorimotor pole and smaller positive age effects distinguishing its association pole. We additionally observed continuous variation in the age at which fluctuation amplitude began to significantly decrease along this dominant organizational axis. When considering regions that showed an initial onset of decline within the age range studied as above, we found that fluctuation amplitude began to decline at a progressively later age in regions ranked higher in the S-A axis ($r = 0.68$, $p_{spin} = 0.00110$). Hence, cortices at the top of the cortical hierarchy exhibit the smallest and latest-onset declines in the amplitude of intrinsic fMRI fluctuations during childhood and adolescence.

Following this initial analysis, we further probed the extent to which maturational trajectories differed as a function of S-A axis rank by mapping the principal spatial axis of fluctuation amplitude development. To accomplish this mapping, we performed a principal component analysis (PCA) on the age fits estimated by regional GAMs (Fig. 1b); this approach considers the entire fluctuation amplitude developmental trajectory rather than only one property of the age fit (e.g., the age at which it starts to decline). The first principal component from this PCA explained 87% of the variance in developmental profiles and can therefore be conceptualized as the principal axis of intrinsic fMRI activity development. This principal developmental axis closely resembled the S-A axis (Fig. 3a). Accordingly, regional loadings onto the principal developmental axis were very highly correlated with regional S-A axis ranks ($r = 0.70$, $p_{spin} < 0.0001$; Fig. 3b), demonstrating that a substantial degree of spatiotemporal variance in developmental profiles was explained by the S-A axis.

The PCA of developmental fits suggests that the spatial and temporal maturation of intrinsic cortical activity conforms to the hierarchical organization of the cortex. In support of this conclusion, we confirmed that principal developmental axis loadings additionally correlated with cortex-wide anatomical[45] ($r = -0.61$), functional[14] ($r = 0.60$), and evolutionary[46] ($r = 0.32$) hierarchies. However, the principal developmental axis was significantly more correlated with the S-A axis than with these three hierarchies, which were defined using unimodal data ($p < 0.001$ for all three statistical tests comparing the magnitude of two dependent, overlapping corrections). Neurodevelopmental trajectories were therefore more parsimoniously captured by the S-A axis, which combines information from all three cortical hierarchies and multiple additional data types. To directly illustrate the manner in which developmental trajectories for fluctuation amplitude evolve from the sensorimotor to the association end of the S-A axis, we divided the axis into 10 decile bins and averaged age fits across all regions in a bin. The continuous spectrum of developmental trajectories visible at the regional level (Fig. 1b) was recapitulated by S-A axis deciles (Fig. 3c).

Development is hierarchical through adolescence

The above results underscore how between the ages of 8 and 23 years, age-related changes in fMRI-indexed intrinsic activity are governed by the brain's S-A axis. We next aimed to elucidate whether this neurodevelopmental pattern was most pronounced during a specific age range or if it was equally present across all ages studied. To explore these possibilities,

we first calculated each cortical region's rate of change in fluctuation amplitude at 1-month intervals between ages 8 and 23 years. Notably, visualizing regional rates of change across the S-A axis (Fig. 4a) confirmed that pre-adolescent increases in fluctuation amplitude were uniquely confined to higher-order association cortices. Using these data, we next performed an age-resolved analysis where, at each 1-month interval, we calculated the correlation between regional rates of amplitude change and regional S-A axis ranks. This procedure generates age-specific correlation values that quantify the extent to which maturational change is spatially ordered along the hierarchy of the S-A axis at a given developmental timepoint. This analysis confirmed a robust correlation between developmental change and S-A axis rank from age 8 to 17 years (Fig. 4b–c). A maximal correlation value of r = 0.68 (95% credible interval: 0.66 to 0.70) was observed at age 15.0 years (95% credible interval: 14.7 to 15.3 years), indicating peak alignment between neurodevelopment and the S-A axis in mid-adolescence. However, following this peak, the correlation between regional age effects and S-A axis position rapidly declined, dropping to 0 by age 19.3 years (95% credible interval: 18.7 to 20.2 years). These findings suggest that the brain's developmental program is hierarchical through late adolescence. Following adolescence, however, there may be a programmed switch in the spatial patterning of subsequent age-related change.

Development results are robust to methodological variation

To ensure that the developmental effects observed were robust to methodological variation and potential confounds, we performed six sensitivity analyses. We evaluated if age-dependent changes in regional fluctuation amplitude were driven by in-scanner head motion, medication use, local cerebral blood flow, regional mean signal intensity, global amplitude differences, or the choice of cortical atlas. In the first two sensitivity analyses, regional GAMs were rerun in the two thirds of the sample with the lowest in-scanner head motion (low motion sample; n = 690; Fig. 5a) and in a sample that excluded individuals with current psychoactive medication use or a history of psychiatric hospitalization (no psychiatric treatment; n = 893; Fig. 5b). In the next two sensitivity analyses, regional GAMs were refit while additionally controlling for regional cerebral blood flow estimated from arterial spin labeling data (vascular control; n = 1,002; Fig. 5c) or regional mean T2* signal intensity (T2* signal control; Fig. 5d). In the final two sensitivity analyses, regional GAMs were refit with whole brain mean-normalized fluctuation amplitude (mean normalization; Fig. 5e) or fluctuation amplitude averaged within Schaefer-400 atlas regions (atlas replication; Fig. 5f) as the dependent variables.

In each of the six sensitivity analyses, region-specific fluctuation amplitude maturational trajectories closely mirrored the developmental fits from the main analysis, with negative age effects observed in most cortices but positive effects seen in select transmodal association cortices. Consequently, regardless of the sample used or controls performed, a cortical region's age effect was fundamentally and significantly (all $p_{spin} < 0.05$) related to its position in the S-A axis (main analysis: r = 0.54, low motion sample: r = 0.56, no psychiatric treatment: r = 0.51, vascular control: r = 0.51, T2* signal control: r = 0.49, mean normalization: r = 0.66, atlas replication: r = 0.43). Furthermore, for all sensitivity analyses, the age-resolved analysis confirmed a strong correlation between the rate of fluctuation amplitude change and S-A axis rank from childhood to late adolescence, with the peak

age of neurodevelopmental alignment to this axis occurring during adolescence. These analyses verify that findings concerning the nature and patterning of age-dependent changes in spontaneous cortical fMRI activity are robust to methodological variation.

Environmental effects vary along the S-A axis in adolescence

During brain maturation, environmental inputs can interact with neurodevelopmental malleability to become cortically embedded, suggesting that variability in children's environments may be reflected in individual differences in development-linked brain changes. We therefore explored whether inter-individual differences in cortical intrinsic fMRI activity may be partly explained by variability in youths' neighborhood environments. Multivariate features of each child's neighborhood socioeconomic environment were summarized using a single previously published factor score[47]. Higher factor scores indicate that an individual lived in a neighborhood with a higher median family income, lower population density, fewer vacant housing lots, a greater percentage of residents who are married, employed, and high school educated, and a lower percentage of residents in poverty (Fig. 6a). We focused on the neighborhood environment, specifically, as the factor score robustly aggregates across a wide range of measures related to the physical, social, and cognitive environment, captures socioeconomic inequality at the societal and systems level, and has been shown to account for individual differences in brain function and behavior beyond the household environment[47,48].

We first modeled linear associations between neighborhood environment factor scores and regional fluctuation amplitude using GAMs while controlling for developmental effects (age) and other covariates (in-scanner motion and sex). Forty-two percent of cortical regions showed a significant association between fluctuation amplitude and the neighborhood environment ($p_{FDR} < 0.05$ in 141 regions). Higher environment factor scores were associated with higher fluctuation amplitude across the association cortex, but with lower fluctuation amplitude nearly exclusively within primary and early sensory and motor cortices (Fig. 6b). This pattern of relationships indicates that youth raised in neighborhoods with higher income, education, and employment rates and with lower population density and poverty tended to have greater amplitude intrinsic fMRI fluctuations in higher-order cortices and lower amplitude fluctuations in modality-specific cortices. Strikingly, environment effects and S-A axis ranks were significantly correlated across the cortical mantle ($r = 0.48$, $p_{spin} < 0.0001$; Fig. 6c), establishing that variation in associations between the neighborhood environment and intrinsic fMRI activity is expressed along the brain's global cortical hierarchy. We attempted to statistically disambiguate between the influence of the neighborhood environment and household socioeconomic position by controlling environment factor score GAMs for parental education, one indicator of individual socioeconomic status. In this specificity analysis, the association between neighborhood environment factor scores and fluctuation amplitude remained significant ($p_{FDR} < 0.05$) in 101 of the original 141 regions and regional environment effects still significantly varied along the S-A axis ($r = 0.54$, $p_{spin} < 0.0001$). Conversely, there were no significant associations between parental education and fluctuation amplitude (all $p_{FDR} > 0.05$), supporting a potentially stronger role for neighborhood-level (dis)advantage than household socioeconomic position.

To better appreciate the nature of associations between the neighborhood environment and fMRI activity amplitude from a developmental perspective, we modeled age-dependent changes in fluctuation amplitude as a function of environment factor score. We visualized developmental trajectories for low and high environment factor scores for deciles of the S-A axis (i.e. Fig. 3c, stratified by factor score). A higher neighborhood environment factor score (indicative of more advantaged socioeconomic circumstances) was associated with a steeper reduction in fluctuation amplitude in sensorimotor regions (deciles 1 and 3) during childhood and adolescence as well as with a greater peak in fluctuation amplitude in association regions (deciles 8 and 10) particularly during mid-adolescence (Fig. 6d). Factor score-stratified developmental trajectories thus suggested that environment effects may be largest and most divergent between sensorimotor and association cortex during adolescence.

To study this possibility further, we divided the sample into child (8–12 years), adolescent (13–17 years), and young adult (18–23 years) groups and quantified regional associations between environment factor scores and fluctuation amplitude at each developmental stage. Regional environment effect estimates were quite correlated across the three groups, suggesting relative stability in associations across development ($r = 0.72$ between child and adolescent t-values, $r = 0.70$ between adolescent and young adult t-values, $r = 0.65$ between child and young adult t-values). However, small differences in regional associations were present across developmental stages (Fig. 6e) and together resulted in environment effect estimates becoming most strongly differentiated across the S-A axis in adolescence. The correlation between regional environment effects and S-A axis ranks was $r = 0.32$ ($p_{spin} = 0.00765$) in children, $r = 0.65$ ($p_{spin} < 0.0001$) in adolescents, and $r = 0.31$ ($p_{spin} = 0.01280$) in young adults.

Given initial evidence that developmental timing may affect the global expression of brain-environment associations, we used GAMs to formally model regional age-by-environment interactions, which estimate how relationships between environment factor scores and fluctuation amplitude vary continuously with age. This approach allowed for the derivation of age-specific environment effect estimates, providing insight into how the magnitude of effects changed over the developmental window studied in individual sensorimotor and association regions (Fig. 6f). Moreover, this approach facilitated a second age-resolved analysis in which we calculated the correlation between age-specific environment effects and S-A axis ranks at 1-month intervals between ages 8 and 23 years (Fig. 6g). The goal of this second age-resolved analysis was to investigate whether subtle changes in regional environment effects contribute to a shift in the global patterning of brain-environment associations with age. This analysis revealed that regional environment effects and regional S-A axis ranks were maximally correlated in adolescence at 15.5 years of age (95% credible interval: 14.4 to 16.6 years), providing convergent results to the grouped developmental stage analysis. The spatial correlation between environment effects and the S-A axis did not significantly differ from zero at the very youngest (< 8.8 years old) and oldest (> 21.0 years old) ages studied. These results collectively suggest that the patterning of brain-environment associations along this principal axis of brain organization is most prominent in adolescence.

DISCUSSION

During embryonic and early postnatal cortical development, developmental programs are spatially and temporally governed by major organizing axes. Cortical arealization is cooperatively controlled by thalamocortical inputs and transcription factors expressed along anterior-medial to posterior-lateral axes[49]. Neurogenesis terminates along an anterior-posterior axis[50]. The alignment of developmental programs with neuroaxes is thus a fundamental element of early cortical development. In the current study, we demonstrate that the maturation of intrinsic cortical activity conforms to the hierarchical S-A axis from ages 8 to 18 years, supporting that this core facet of development extends to childhood and adolescence. Specifically, we observed that declines in the amplitude of intrinsic fMRI activity are temporally coupled to the increasing expression of a plasticity-limiting factor and temporally staggered along the S-A axis of cortical organization. We additionally found that the S-A axis captures not only inter-regional variation in maturational profiles, but also variation in the effects of children's developmental environment on intrinsic fMRI activity. Together, these results provide evidence of a hierarchical axis of neurodevelopment in youth.

Intrinsic neural activity has a profound influence on the immature brain, impacting neuron survival, circuit wiring, topographic map formation, synaptic connectivity, and overall cortical volume[18,51–53]. Prominent changes in the prevalence and patterning of this activity occur during development, engendered by shifts in the maturity of the cortex and in the level of cortical plasticity. Here, we identified prolonged declines in fMRI fluctuation amplitude, an in vivo measure sensitive to intrinsic cortical activity, throughout the protracted course of human neurodevelopment. Moreover, we observed substantial inter-regional heterochronicity in periods of decline, with fluctuation amplitude beginning to decline around 8–12 years of age in unimodal sensory and motor regions, 13–16 years in many association cortices, and 18–22 years in prefrontal transmodal cortices. These region-specific windows of declining fluctuation amplitude occur after peak gray matter volume is obtained[5] and coincide with regional windows of extensive synaptic pruning[10]. In addition, we demonstrated that each region's onset of decline in fluctuation amplitude was linked to its period of maximal intracortical myelin growth. Maturational refinement of this non-invasive functional measure is thus temporally linked to developmental changes in multiple indicators of shifting circuit plasticity, suggesting the presence of a graded axis of neurodevelopmental plasticity during childhood and adolescence.

Indeed, in support of our proposed framework on developmental chronology[4], we found that regional differences in maturational profiles were systematically explained by the asynchronous patterning of developmental change across the S-A axis. Regional developmental trajectories diverged in a continuous fashion across this axis, in a manner that suggests a maturational sequence progresses along the brain's global cortical hierarchy with age. This underscores that the S-A axis can be considered both a dominant spatial feature axis and a primary neurodevelopmental axis, and intimates that spatial feature variability may in part emerge from temporal developmental variability[4,50]. Recent work has shown that cortical microstructure[9] and functional connectivity[7] increasingly differentiate across the S-A axis during late childhood and adolescence, when development is maximally organized by this axis. Hence, one main outcome of hierarchical development may be the

strengthening of variation along the S-A axis with a consequent strengthening of the cortex's hierarchical topography[4].

Although this non-invasive imaging study could not establish the mechanisms underlying the sensorimotor-to-associative sequence of fMRI activity refinement, prior work suggests that it may be produced by the hierarchical maturation of plasticity-regulating structural and chemical features. Key plasticity-regulating processes include the growth of intracortical myelin[25,54], the strengthening of parvalbumin interneuron signaling[24,54], and the assembly of perineuronal nets[17,55]. These processes elicit transitions in the prevalence, synchronicity, and recorded amplitude of spontaneous activity[17,23,44,56], indicating that they could possibly contribute to developmental changes in fMRI activity amplitude. In the adult cortex, the cortical distribution of parvalbumin interneurons is coupled to regional differences in fMRI fluctuation amplitude, with parvalbumin interneuron-associated genes accounting for an enriched degree of heritable variance in this measure[56]. In the developing cortex, cortical myelin and perineuronal nets preferentially form around parvalbumin interneurons[17,55,57], limiting developmental plasticity while simultaneously altering a circuit's excitation:inhibition ratio and the production of intrinsic activity[11,54]. Critically, it has been established that cortical myelin[8,42] and parvalbumin interneurons[11,16,58] mature earlier in sensory cortices and later in association cortices, indicating that their temporal development parallels the developmental reductions in the amplitude of intrinsic fMRI activity characterized here. The amplitude of intrinsic fMRI activity also uniquely increased in transmodal cortices in adolescence (frequently until 13–17 years) suggesting that a functional signature of more highly malleable cortices increases in association areas in this developmental window. The neurobiological events that could contribute to late increases in association cortex plasticity in the human brain have yet to be identified. Candidate events identified in animal studies include slower degradation of molecules that can delay the onset of plasticity (e.g., polysialic acid[54], histone deacetylases[16]) or late increases in plasticity facilitators (e.g., brain-derived neurotrophic factor[54], thalamocortical inputs[59], homeoprotein Otx2[54]).

It has been hypothesized that the same external inputs may exert differential influences on the human brain depending on developmental timing, due to age-dependent changes in the distribution of cortical plasticity; the present work provides empirical support for this hypothesis. Specifically, we studied relationships between individual differences in intrinsic activity amplitude and environment factor scores; these scores index disparities in neighborhood-level socioeconomic conditions that should be recognized as a manifestation of systemic wealth and education inequity that is rooted in structural racism and racial inequity[60]. We found that youth living in neighborhoods with greater poverty, unemployment rates, and population density exhibited reduced fluctuation amplitude across the association cortex—most prominently, a reduced peak in amplitude in transmodal cortex during mid-adolescence. Yet, youth from more disadvantaged environments also had higher amplitude intrinsic fMRI activity in unimodal sensory and motor cortices. Together, these opposing environment effects in sensorimotor and association cortex indicate that greater environmental deprivation is associated with diminished differentiation of a putative functional plasticity signature across the maturing cortex. We speculate that this association could reflect reduced versus accelerated development of plasticity-restricting features such

as myelin in sensorimotor and association cortices, respectively, in youth from poorer socioeconomic environments[61].

Significantly, the cortical expression of brain-environment associations was not uniform across the entire age range studied. An age-resolved analysis revealed that environment effects diverged most between sensorimotor and association cortex during adolescence —coincident with when cortex-wide differences in developmental change were most hierarchically organized. In fact, both developmental and environmental effects exhibited maximal variation across the cortex's S-A axis at 15 years of age. This temporal concurrence uncovers interdependence between ongoing neurodevelopmental refinement and environmental influences, further suggesting that the effects of the environment on the youth brain depend on developmental stage. Our analyses of youths' neighborhood environments thus provide data consistent with the hypothesis that environmental influences are both sensitive to and capable of refining a cortical area's current developmental state.

Several limitations and possible direct extensions of this work should be highlighted. First, this was a cross-sectional investigation of neurodevelopment in youth. Future investigations with longitudinal study designs could characterize within-individual changes in cortical intrinsic activity as well as the effects of the environment on the pace of an individual's development. Longitudinal studies will also be better suited to examine temporal precedence between developmental refinement of intrinsic fMRI activity and maturation of plasticity-regulating features. Second, we used resting-state functional MRI to study intrinsic cortical activity, however the BOLD signal is sensitive to neural, vascular, and respiratory factors. While sensitivity analyses aimed at assessing and mitigating these factors provided highly convergent results, future studies using more direct measures of neural activity will therefore be helpful for extending the present findings. Third, it is difficult to directly establish the extent to which age-related changes in non-invasive neuroimaging measures represent changes in developmental plasticity versus other processes, given that there is no gold-standard or singular measure of cortical plasticity in the human brain. To address this challenge, we studied an fMRI-derived measure that is modulated by changing the activity of cells that drive developmental plasticity[16,34,56], is enhanced by behaviorally inducing plasticity[33,35], and, as shown here, is refined during development in tandem with a biological regulator of plasticity. Fourth, only a coarse measure of pubertal stage was available in this sample, and it was only collected in individuals 10 years of age and older. This limited our ability to fully ascertain whether regional fluctuation amplitude was influenced by puberty or hormone levels, especially in the youngest participants. Rodent studies have shown that pubertal hormones can affect synaptic pruning and inhibitory signaling in association cortex[62], highlighting this as an area for further investigation. Fifth, we aggregated a set of interrelated neighborhood variables into one factor score, precluding inference about specific proximal or distal causes of the brain-environment associations observed in these data. Potential causes may involve neighborhood features that are socioeconomically stratified and socio-politically determined including access to physical resources, healthcare, and education, exposure to environmental enrichment and community programs, or experiences of psychological safety and chronic stress. Developing a more nuanced understanding of the causes and behavioral correlates of these environment

effects may ultimately help to inform interventions or policies that equitably support healthy child neurodevelopment across socioeconomic circumstances.

The present study demonstrates that during childhood and adolescence, the spatiotemporal patterning of developmental change in intrinsic cortical fMRI activity coheres with a hierarchical axis of cortical organization. The observed refinements in fMRI fluctuations lend support to the theory that shifts in circuit plasticity temporally progress along this axis, calling for studies that can mechanistically test for neurobiological events driving a S-A gradient of neurodevelopment. Such events may include the maturation of neurochemical and structural plasticity-regulating features as well as successive expression of molecules that can orchestrate developmental timing, for example circadian clock genes and temporally organized transcription factors[16,63,64]. Given the relevance of the S-A axis for understanding cortical development in childhood and adolescence, future work should explore whether this and other major organizing axes (e.g., anatomical axes) play a role in cortical refinement during infancy and early childhood. Studies of the infant brain have shown that developmental change in thalamocortical structural connectivity and cortico-cortical functional connectivity is more pronounced within sensorimotor than association cortex, suggesting maturational relevance of the S-A axis in the first years of life[65]. Continued discovery of temporal axes of neurodevelopment across human's multi-decade maturational course will help elucidate how plasticity is distributed across brain regions at different developmental stages. Such insights into the temporal patterning of plasticity will facilitate an understanding of how the effects of experience and the environment on the brain change as cortical malleability is refined, and may thus ultimately help to guide interventions in youth that align with each child's neurotemporal context.

METHODS

Participants

Participants were recruited as part of the Philadelphia Neurodevelopmental Cohort[66], a community study of child and adolescent brain development. Demographic, clinical, environmental, and neuroimaging data from 1,033 youth were included in the present cross-sectional study. Study sample demographics include an age range of 8 to 23 years (mean age = 15.7 ± 3.3 years), a sex distribution of 467 males and 566 females (sex was self-reported; intersex was not assessed), and a race and ethnicity distribution that was 0.3% American Indian or Alaskan Native, 0.7% Asian, 41% Black or African American, 11% identifying as multiracial, and 47% White. All participants over the age of 18 gave written informed consent prior to study participation. Participants under the age of 18 gave informed assent with written parental consent. All individuals received monetary compensation for participation in the study. All study procedures were approved by the Institutional Review Boards of the University of Pennsylvania and the Children's Hospital of Philadelphia.

MRI data acquisition

T1-weighted structural MRI and resting-state functional MRI data were used in the present study. All MRI scans were acquired on the same 3T Siemens TIM Trio scanner (software version VB17) at the University of Pennsylvania with a 32-channel head coil. T1-weighted

structural images were acquired with a magnetization-prepared rapid acquisition gradient-echo (MPRAGE) sequence with the following parameters: repetition time = 1810 ms, echo time = 3.51 ms, inversion time = 1100 ms, flip angle = 9 degrees, field of view = 180 × 240 mm, matrix = 192 × 256, slice number = 160, voxel resolution = 0.94 × 0.94 × 1 mm. Resting-state functional images were acquired with a single-shot, interleaved multi-slice gradient-echo echo planar imaging (GE-EPI) sequence with the following parameters: repetition time = 3 s, echo time = 32 ms, flip angle = 90 degrees, field of view = 192 × 192 mm, matrix = 64 × 64, slice number = 46, voxel resolution = 3 mm^3, volumes = 124. To enable susceptibility distortion correction of resting-state functional images, a map of the main magnetic field (i.e., a B0 field map) was additionally collected using a dual-echo, gradient-recalled echo (GRE) sequence with the following parameters: repetition time = 1000 ms, echo time 1 = 2.69 ms, echo time 2 = 5.27 ms, flip angle = 60 degrees, field of view = 240 × 240 mm, matrix = 64 × 64, slice number = 44, voxel resolution = 3.8 × 3.8 × 4 mm.

MRI data processing

T1-weighted images and resting-state functional MRI timeseries were processed with fMRIPrep 20.2.3[67]. The T1-weighted image was corrected for intensity non-uniformity with Advanced Normalization Tools[68] (ANTs; 2.3.3) N4BiasFieldCorrection, skull stripped with a Nipype (1.6.1) implementation of the ANTs brain extraction workflow, tissue segmented with FSL (5.0.9) fast, and used for cortical surface reconstruction with FreeSurfer (6.0.1)[69]. The T1-weighted image was additionally non-linearly registered to the MNI152 T1 template (volume-based spatial normalization) with antsRegistration.

To preprocess functional scans, a skull-stripped reference BOLD volume was first generated and a B0 fieldmap was co-registered to this reference volume. The B0 field map was estimated based on the phase-difference map calculated with the dual-echo GRE sequence, converted to a displacements field map with FSL's fugue and SDCflow tools, and used for susceptibility distortion correction of the reference BOLD volume. The susceptibility corrected BOLD reference was then rigidly co-registered (6 degrees of freedom) to the T1 reference using boundary-based registration implemented with FreeSurfer's bbregister. The functional MRI timeseries were slice-time corrected using 3dTshift from AFNI 20160207 and then resampled onto their original, native space by applying a single, composite transform to correct for susceptibility distortions and for in-scanner head motion. Head motion parameters were calculated with respect to the reference BOLD volume prior to any spatiotemporal filtering using FSL mcflirt; six rotation and translation parameters were calculated. BOLD timeseries were additionally resampled into standard space, generating preprocessed timeseries in the MNI152NLin6Asym T1 template, and onto the fsaverage surface. Finally, to project functional timeseries onto the fsLR cortical surface for study analyses, grayordinates files containing 32k vertices per hemisphere were generated using the highest-resolution fsaverage as an intermediate standardized surface space. Volumetric resampling was performed using antsApplyTransforms, configured with Lanczos interpolation to minimize the smoothing effects of other kernels. Surface resampling was performed using FreeSurfer's mri_vol2surf.

fMRIPrep was additionally used to estimate the following 36 confounds from the preprocessed timeseries: six head motion parameters; three region-wise global signals (mean cerebrospinal fluid, white matter, and whole brain signals); temporal derivatives of the six head motion parameters and the three global signal estimates; and quadratic terms for the motion parameters, tissue signals, and their temporal derivatives[70,71]. These confound matrices were utilized within xcp_d 0.0.4, which is an extension of the top-performing eXtensible Connectivity Pipeline (XCP) Engine[70,71] specifically developed to mitigate motion-related artifacts and noise in resting-state functional MRI data from developmental samples. With xcp_d, preprocessed functional timeseries on the fsLR cortical surface underwent nuisance regression using the 36 confounds listed above. Confounds were regressed using linear regression as implemented in Scikit-Learn (0.24.2).

Fluctuation amplitude quantification

To calculate fluctuation amplitude, defined as the power of low frequency fMRI recordings, processed fsLR surface BOLD timeseries were first transformed from the time domain to the frequency domain and a power spectrum was generated in the 0.01–0.08 Hz range. The mean square root of the power spectrum was then calculated. The mean square root represents the average amplitude (intensity) of time-varying resting-state BOLD fluctuations within this low frequency band[32]. Of note, the fluctuation amplitude measure used here is analogous to other commonly used spectral- or variability-based BOLD measures, including the amplitude of low frequency fluctuations (ALFF) and resting-state functional amplitude (RSFA).

Fluctuation amplitude was quantified at the vertex-level with xcp_d 0.0.4 and then parcellated with fsLR surface atlases to provide mean fluctuation amplitude within individual cortical regions. The HCP multimodal atlas[72] was used for all primary analyses and the Schaefer-400 atlas[73] was used for a sensitivity analysis. Parcellation was conducted in R with the *ciftiTools* package[74] utilizing Connectome Workbench 1.5.0. Fluctuation amplitude was not analyzed within cortical regions that exhibited low signal to noise ratio (SNR) in >= 25% of their assigned vertices. Low SNR vertices were defined identically to our prior work[75] as vertices with an average (across-participant) BOLD signal < 670 after normalizing signal to a mode of 1000. Twenty-four parcels located within the orbitofrontal cortex and the ventral temporal lobe were excluded from both the HCP multimodal atlas and the Schaefer-400 atlas.

MRI sample construction

The study sample used in the present work is comprised of individuals who received an MRI scan as part of the Philadelphia Neurodevelopmental Cohort. No statistical methods were used to pre-determine the sample size of the Philadelphia Neurodevelopmental Cohort as this was designed as a large, publicly available, community data resource, but the sample size is similar to that reported in previous publications of youth brain development[42,48,66]. 1,374 individuals in the Philadelphia Neurodevelopmental Cohort had T1-weighted images, B0 field maps, and identical parameter[76] resting-state functional MRI scans available and were considered for inclusion in this study. From this original sample of n = 1,374, 120 individuals were excluded from the study due to medical problems that could impact

brain function or incidentally encountered abnormalities of brain structure. Data from 202 additional participants were excluded due to low quality T1-weighted images and FreeSurfer reconstructions (n = 23) or high in-scanner head motion (n = 179). As in our prior work, high in-scanner head motion was defined as a mean relative root mean squared framewise displacement > 0.2 mm during the functional scan. Using data from the remaining sample (n = 1,052), we identified fluctuation amplitude outliers at the regional level based on a cut off of ± 4 standard deviations from the mean. Individuals with outlier data in more than 5% of cortical regions (n = 19) were excluded, producing the final study sample of 1,033 individuals. Participants from this final study sample were not assigned to separate experimental groups or conditions, thus data collection and analysis did not involve randomization or blinding.

Characterizing developmental effects

Generalized additive models—All statistics were carried out in R 4.0.2. In order to flexibly model linear and non-linear relationships between fluctuation amplitude and age, we implemented GAMs (semi-parametric, additive models) using the *mgcv* package in R[77]. GAMs were fit with regional fluctuation amplitude as the dependent variable, age as a smooth term, and sex and in-scanner head motion as linear covariates. Models were fit separately for each parcellated cortical region using thin plate regression splines as the smooth term basis set and the restricted maximal likelihood approach for smoothing parameter selection. The GAM smooth term for age produces a spline, or a smooth function generated from a linear combination of weighted basis functions, that represents a region's developmental trajectory. To prevent overfitting of the spline, we set the maximum basis complexity (k) to 3 to limit the number of basis functions that could be used to estimate the overall model fit. A value of k = 3 was chosen over higher values (i.e., k = 4–6) given that this basis complexity resulted in the lowest model Akaike information criterion (AIC) for the majority of cortical regions. Statistical tests of the k-index[77], which estimate the degree of unaccounted for, non-random pattern in the residuals, confirmed that this basis dimension was sufficient.

For each regional GAM, the significance of the association between fluctuation amplitude and age was assessed through an analysis of variance (ANOVA) that compared the full GAM model to a nested, reduced model with no age term. A significant result indicates that the residual deviance was significantly lower when a smooth term for age was included in the model, as assessed with the chi-square test statistic. We corrected ANOVA *p*-values across all region-wise GAMs using the false discovery rate (FDR) correction and set statistical significance at $p_{FDR} < 0.05$ corrected. For each regional GAM with a significant age smooth term, we furthermore identified the specific age range(s) wherein fluctuation amplitude was significantly changing through the *gratia* package in R. Age windows of significant change were identified by quantifying the first derivative of the age smooth function (Δ fluctuation amplitude / Δ age) using finite differences and determining when the simultaneous 95% confidence interval of this derivative did not include 0[78] (two-sided). To establish the overall magnitude and direction of the association between fluctuation amplitude and age, which we refer to throughout as a region's overall age effect, we calculated the partial R^2 between the full GAM model and the reduced model (effect

magnitude) and signed the partial R^2 by the sign of the average first derivative of the smooth function (effect direction).

For each cortical region, we additionally tested the effects of participant sex and pubertal stage on fluctuation amplitude development. We first assessed whether the developmental trajectories of fluctuation amplitude differed between males and females by testing the significance of a factor-smooth interaction term added to the main GAM model (i.e., an age-by-sex interaction that allowed age-dependent changes to vary by sex). To assess the potential influence of participant pubertal stage, we added a three-level ordered factor for pubertal stage (with levels for pre-pubertal, mid-pubertal, and post-pubertal) to the main GAM models. Participants self-reported their pubertal stage by viewing pictorial representations and text descriptions of the five Tanner stages of pubic hair growth and reporting which best matched their own development of secondary sex characteristics. Following our prior work in this same sample[79], we considered Tanner stages 1–3 as "pre-pubertal", Tanner stage 4 as "mid-pubertal" and Tanner stage 5 as "post-pubertal". Self-reporting of Tanner staging was only conducted in participants ages 10 and older (n = 949; 518 female). As a result, there were fewer pre-pubertal participants (n = 176, Tanner stages 1–3) than mid-pubertal (n = 283, Tanner stage 4) and post-pubertal (n = 490, Tanner stage 5) participants. We evaluated whether pubertal stage explained significant variance in fluctuation amplitude above and beyond age in each region by using an ANOVA to compare the full GAM model (with the pubertal stage factor) to a reduced model that did not include pubertal information. We corrected *p*-values for multiple comparisons across region-wise GAMs within sex and pubertal stage analyses using FDR correction.

Associations with cortical myelin development—We formally assessed whether the development of intrinsic fMRI activity amplitude was spatially and temporally related to the development of an imaging measure sensitive to intracortical myelin content. Cortical myelin development was previously comprehensively characterized by Baum et al. (2022)[42] using T1w/T2w surface-based myelin mapping in a sample of 628 youth ages 8 to 21 years (336 female) who had data collected as part of the Human Connectome Project in Development. Using high resolution (0.8 mm^3) T1-weighted and T2-weighted images, HCP processing pipelines, and state of the art methods for B1+ transmit field bias correction and partial volume reduction, Baum et al. (2022)[42] investigated the maturational trajectory of increases in the T1w/T2w ratio in each cortical region. In this investigation, the authors fit region-specific GAMs with a smooth term for age using thin plate regression splines as the smoothing basis, paralleling the present work. GAMs included covariates for sex, scanner, and B1+ transmit field correction-related variables, following current best practices for statistically comparing the T1w/T2w ratio across individuals.

To test if the extent to which fluctuation amplitude changed with age was related to the degree to which cortical myelin content changed with age, we calculated the correlation coefficient between the two distinct age effects: those calculated from regional fluctuation amplitude GAMs and those calculated from regional T1w/T2w ratio GAMs reported by Baum et al. (2022)[42]. As in the present work, T1w/T2w ratio age effects were determined by a partial R^2 derived by comparing the full GAM model to a reduced model with no smooth term for age. The association between fluctuation amplitude age effects and T1w/T2w

ratio age effects was quantified with a Spearman's correlation, a non-parametric, rank-based correlation test that does not assume normality. A Spearman's correlation was also used to evaluate whether there was temporal correspondence between the development of fluctuation amplitude and the T1w/T2w ratio across the cortex. Specifically, we calculated the correlation coefficient between the age at which fluctuation amplitude began to significantly decrease in each region and the age at which the T1w/T2w ratio maximally increased in each region. The age at which fluctuation amplitude began to significantly decrease was the youngest age at which the first derivative of the age smooth function was significantly negative. The age at which the T1w/T2w ratio had a maximal rate of increase was the age at which the first derivative of the age smooth function was maximal.

Alignment with the sensorimotor-association axis—This work set out to test the overarching hypothesis that neurodevelopmental patterns are organized by the S-A axis during childhood and adolescence. We therefore examined whether patterns of fluctuation amplitude maturation aligned with the S-A axis derived in our prior work[4]. The S-A axis was derived by averaging rank orderings of ten cortical feature maps that exhibit systematic variation between lower-order sensorimotor cortices, middle-order unimodal and multimodal cortices, and higher-order heteromodal and paralimbic association cortices[4]. These maps include: the functional hierarchy delineated by the principal gradient of functional connectivity[14], the evolutionary hierarchy defined by macaque-to-human cortical areal expansion[46], the anatomical hierarchy as quantified by the adult T1w/T2w ratio[45], allometric scaling calculated as local areal scaling with scaling of total brain size[80], aerobic glycolysis measures of brain metabolism[81], cerebral blood flow measures of brain perfusion[79], gene expression patterning indexed by the principal component of brain-expressed genes[45], a primary mode of brain function characterized by the principal component of NeuroSynth meta-analytic decodings[82], a histological gradient of cytoarchitectural similarity developed using the BigBrain atlas[83], and cortical thickness measured by structural MRI. The resulting S-A axis represents a dominant, large-scale motif of cortical organization that captures the stereotyped patterning of cortical heterogeneity from primary visual, somatosensory, and motor regions (lowest ranks in the S-A axis) to transmodal frontal, temporal, and parietal association regions (highest ranks in the S-A axis).

We performed the following analyses to ascertain whether the development of fluctuation amplitude is related to the S-A axis. Using Spearman's correlations, we evaluated associations between cortical regions' S-A axis ranks and both 1) their magnitude of fluctuation amplitude development (signed GAM partial R^2) and 2) the age at which their fluctuation amplitude began significantly decreasing (first significant negative derivative). We next conducted a PCA on regional developmental trajectories. The goal of this PCA was to visualize the spatial axis that explained the greatest variance in how an in vivo measure of cortical intrinsic activity changed with age. The input to the PCA was region-wise age fits (zero-averaged smooth function estimates). The first principal component generated by this PCA contained regional loadings that capture differences in maturational patterns across one low-dimensional embedding. We quantified the similarity between the first principal component (loadings) and the cortex's S-A axis[4], anatomical hierarchy[45], functional hierarchy[14], and evolutionary hierarchy[46] with independent Spearman's correlations. We

additionally assessed whether the correlation with the S-A axis was significantly greater in magnitude than correlations with the three aforementioned hierarchies using a statistical test for comparing two dependent, overlapping correlations that utilizes a back-transformed average Fisher's Z procedure; tests were executed using the *cocor* package in R[84] (*hittner2003* test; two-sided).

Finally, we implemented an age-resolved analysis to evaluate if the development of fluctuation amplitude aligned with the S-A axis throughout the entire developmental window studied. For this analysis, we computed across-region Spearman's correlations between S-A axis rank and the first derivative of the GAM age spline estimated at 200 ages between 8 and 23 years—producing 200 age-specific correlations. In other words, we quantified the relationship between a region's fluctuation amplitude rate of change and its position in the S-A axis at 200 age increments, allowing us to study changes in the extent of S-A axis alignment over the course of development. We determined a correlation coefficient point estimate as well as a 95% credible interval for these age-specific correlation values at all 200 age increments. To do so, we sampled from the posterior distribution of each region's fitted GAM 10,000 times, generating 10,000 simulated age smooth functions and corresponding derivatives. We then repeated the process of correlating S-A axis rank with the first derivative of the age smooth function at each of the 200 ages for all 10,000 posterior draws, generating a sampling distribution of possible correlation values at each age increment. This distribution was used to calculate the median correlation value (point estimate) and the 95% credible interval of correlation values at each age increment. In addition, the sampling distribution of age-specific S-A axis correlation values was used to identify the age at which fluctuation amplitude development maximally aligned with the S-A axis and the youngest age at which no alignment to the axis was observed. To discover ages of maximal and null alignment, we calculated the age at which the axis correlation was largest as well as the first age at which the correlation equaled 0 for all 10,000 draws. For both measures, the median age across all draws and a 95% credible interval was calculated.

Sensitivity analyses—We performed a series of sensitivity analyses to confirm that the developmental effects observed were not being driven by potentially confounding factors including in-scanner head motion, psychiatric medication use, cerebrovascular perfusion, BOLD signal intensity, global amplitude effects, or the atlas used for cortical parcellation. For each sensitivity analysis, regional GAMs were refit either in a reduced sample (head motion and psychiatric medication analyses), in the full sample but with an additional model covariate (vascular and BOLD signal intensity analyses), or in the full sample with a modified dependent variable (global amplitude normalization and cortical atlas analyses). GAM-derived fluctuation amplitude trajectories were then visualized and developmental alignment with the S-A axis was assessed.

The first sensitivity analysis was conducted with a low motion sample to mitigate the potential confounding effect of in-scanner head motion on fluctuation amplitude. From the main study sample of 1,033 individuals, we excluded 343 individuals with a mean relative root mean squared framewise displacement > 0.075, retaining a low motion sample of n = 690 (ages 8–23 years; mean age = 16.1 years; 395 female). The second sensitivity analysis was carried out to ensure that psychotropic medication use, which was more frequent among

older study participants, did not explain the age-related changes in fluctuation amplitude. GAMs were refit after removing all participants (n = 140) from the original sample of 1,033 individuals that reported current psychoactive medication use or a history of psychiatric hospitalization (remaining n = 893; ages 8–23 years; mean age = 15.6 years; 507 female).

The third sensitivity analysis aimed to address the fact that the hemodynamic BOLD signal has vascular contributions. Prior work has demonstrated that measures of BOLD fluctuation amplitude contain substantial physiological information not attributable to vascular properties such cerebrovascular reactivity, rigidity, and blood flow[85]. Nonetheless, we still evaluated whether changes in vascular reactivity or cerebral perfusion with age could potentially be contributing to our developmental findings concerning fluctuation amplitude. We approached this evaluation by directly controlling for each participant's regional cerebral blood flow, a measure of local blood perfusion, in region-wise GAMs. Cerebral blood flow was estimated from arterial spin labeling (ASL) data collected from participants with a pseudo-continuous ASL (pCASL) sequence with the following acquisition parameters: repetition time = 4000 ms, echo time = 2.9 ms, voxel resolution = 2.29 × 2.29 × 6 mm, label duration = 1500 ms, post label delay = 1250 ms, 40 paired label and control acquisition volumes. Data were processed using ASLPrep version 0.2.7 using the analysis pipeline reported in Adebimpe et al. (2022)[86]. Basic cerebral blood flow maps were generated and parcellated with the HCP multimodal atlas. Thirty-one participants included in the main study sample did not have ASL data available thus this vascular control analysis was performed using data from the remaining 1,002 participants (ages 8–23 years; mean age = 15.7 years; 552 female).

The fourth sensitivity analysis was undertaken to rule out the possibility that inter-individual differences in regional mean BOLD signal intensity, rather than BOLD fluctuations per se, could account for our findings. In the full study sample (n = 1,033), region-specific GAMs were refit while adding regional mean BOLD signal (i.e., the average T2* signal from minimally preprocessed functional timeseries) as an additional control covariate. Regional mean BOLD signal was calculated from parcellated fsLR surface BOLD timeseries generated with fMRIPrep by averaging the BOLD signal intensity in each parcellated cortical region across all volumes; this measure was calculated prior to regression of confounding signals.

The fifth sensitivity analysis used mean normalized fluctuation amplitude as the dependent variable in all regional GAMs to examine the extent to which region-specific changes in fluctuation amplitude with age occurred above and beyond changes in global mean fluctuation amplitude. This sensitivity analysis was motivated by prior work that normalized local brain measures by a whole-brain mean to reduce inter-individual differences in global values[45]. It furthermore accounts for potential global differences in the scale of the BOLD signal across scans. Mean normalized fluctuation amplitude was quantified for all participants (n = 1,033) by dividing an individual's fluctuation amplitude in each parcellated cortical region by the average fluctuation amplitude computed across all cortical regions. Notably, because whole-brain mean fluctuation amplitude declined across the age range studied, regional trajectories in this sensitivity analysis represent regional age-related decreases or increases relative to this global change.

The sixth and final sensitivity analysis was implemented to verify that the hierarchical sequence of fluctuation amplitude maturation would be observed when using a different atlas for cortical parcellation. As described above, vertex-wise fluctuation amplitude data in fsLR surface space were parcellated with the Schaefer-400 atlas. GAMs were fit using data from the main study sample of 1,033 individuals for each Schaefer atlas region.

Characterizing environmental effects

Neighborhood environment factor scores—To ascertain whether children's developmental environment may influence intrinsic cortical activity patterns, we investigated associations between spontaneous BOLD fluctuations and neighborhood environment factor scores that index differences in neighborhood-level socioeconomic circumstances. The derivation of these factor scores has been previously explained in detail[47]. Briefly, geocoded information about each individual's neighborhood environment was extracted using their home address and the census-based American Community Survey. The first factor from an exploratory, two-factor factor analysis conducted on census variables by Moore et al. (2016)[47] is used in the present study. This neighborhood environment factor score had positive loadings for the percent of residents who are married (loading = 0.85), median family income (0.82), the percent of residents with a high school education (0.74), the percent of residents who are employed (0.68), and median age (0.61) as well as negative loadings for the percent of residents in poverty (−0.86), population density (−0.71), and the percent of houses that are vacant (−0.60), and a weak loading for the percent of residents who are female (−0.26). There was no correlation between age and neighborhood environment factor scores ($r = 0.01$).

Generalized additive models—GAMs were used to investigate whether variability in youths' neighborhood environments was associated with variability in regional fluctuation amplitude. We first used GAMs to resolve age-independent main effects of the neighborhood environment by modeling environment factor scores as a linear independent variable. For each region in the HCP multimodal atlas, a GAM was fit with fluctuation amplitude as the dependent variable, age as a smooth term, and sex, in-scanner motion, and the environment factor score as linear covariates. These main effect models thus identify linear associations between factor scores and regional fluctuation amplitude across the entire developmental age range studied. The *t*-value associated with the factor score term in each GAM represents the magnitude and direction of the regional fluctuation amplitude-neighborhood environment association. The significance of this association was assessed with an ANOVA that compared the full GAM model to a reduced model without the environment factor score term; ANOVA *p*-values were FDR corrected across all region-wise GAMs.

The main effect GAMs described above were also used in a follow-up specificity analysis. The specificity analysis was conducted to evaluate whether the observed environmental effects were specific to youths' neighborhood environments or could be better accounted for by the household-level socioeconomic environment. To investigate this, parental education—one indicator of household socioeconomic position—was included as an additional linear covariate in regional GAMs. For each region, the significance (FDR-corrected) of both

the environment factor score term and the parental education term was assessed using ANOVAs as indicated above. Parental education was defined as the average years of education obtained by both parents (when data was available, n = 943) or by one parent (n = 83). Parental education information was not available for seven participants who were thus removed from this secondary analysis. Parental education was used as a proxy for household-level socioeconomic position as other socioeconomic measures (e.g., household income or parental occupational status) were not collected, though we note that individual socioeconomic position may be more robustly operationalized by combining multiple measures.

After assessing the specificity of effects to the neighborhood environment, we conducted two complementary analyses aimed at understanding whether the global cortical patterning of associations between fluctuation amplitude and neighborhood environment factor scores varies by age. We first examined main effect associations between the factor scores and regional fluctuation amplitude in groups of participants at different developmental stages. The study sample was divided into child (8–12 years; n =175; 94 female), adolescent (13–17 years; n = 405; 225 female), and young adult (18–23 years; n = 299; 167 female) groups and region-wise main effect environment GAMs (as described above) were fit independently in each group. Regional environment factor score *t*-values were then obtained for each group. This developmental stage analysis suggested that associations between the neighborhood environment and fluctuation amplitude may vary by age in some regions, producing changes in the cortical expression of environment effects. To further explore this possibility, we examined regional age-by-environment interactions, which explicitly model how associations between the neighborhood environment and regional fluctuation amplitude change continuously with age. In each region, we fit a varying coefficient GAM with fluctuation amplitude as the dependent variable; predictors included an age-by-factor score interaction term, a smooth term for age, and control covariates including sex and in-scanner motion. These models use data from the entire sample and allow the linear association between environment factor scores and regional fluctuation amplitude to vary as a smooth function of age. Region-wise varying coefficient GAMs were utilized for two main objectives. First, we used these models to generate predicted trajectories of fluctuation amplitude development for low (10^{th} percentile) and high (90^{th} percentile) factor scores for every region. We then averaged trajectories for low and high factor scores independently within deciles of the S-A axis for visualization purposes. Second, we used these models to quantify age-specific environment effects in each region. Age-specific environment effects were computed as the slope of the linear association between fluctuation amplitude and environment factor scores at a given age (Δ fluctuation amplitude / Δ factor score). The organization of age-specific environment effects along the S-A axis was then examined across development (detailed further below).

Alignment with the sensorimotor-association axis—To first assess whether the main effects of the environment on fluctuation amplitude were systematically related to the S-A axis, we tested for an association between neighborhood environment factor score *t*-values and S-A axis ranks using a Spearman's correlation. Correlations between *t*-values and S-A axis ranks were quantified for the primary analysis as well as for the

follow-up specificity and developmental stage analyses. To additionally understand how the spatial correlation between regional brain-environment associations and S-A axis ranks changed across the entire developmental window studied, we conducted an age-resolved environmental effects analysis. Akin to the age-resolved development analysis, we computed across-region Spearman's correlations between S-A axis ranks and age-specific environment effects (varying coefficient model slopes) at 200 ages between 8 and 23 years. We determined a correlation coefficient point estimate (median correlation value) as well as a 95% credible interval for these age-specific correlation values from 10,000 draws from the posterior distribution of each region's fitted varying coefficient GAM. As in the development analysis, we also identified the age at which variation in environment effects was maximally captured by the S-A axis; a point estimate and a 95% credible interval for the age of maximal S-A axis correlation was calculated.

Spin-based spatial permutation testing

Cortical data often exhibit distance-dependent spatial autocorrelation that can inflate the significance of correlations between two cortical feature maps. To mitigate this issue, we assessed the significance of each Spearman's correlation that compared two whole-brain cortical feature maps with non-parametric, spin-based, spatially-constrained rotation tests, or "spin tests"[87]. Spin tests compute a *p*-value (denoted p_{spin}) by comparing the empirically observed correlation to a null distribution of correlations obtained by randomly spatially iterating (spinning) one of the two cortical feature maps. In particular, spin tests generate a null by rotating spherical projections of one feature map while maintaining its spatial covariance structure. The direction of the empirical Spearman's correlation can be positive or negative; the *p*-value for the correlation is quantified as the number of times the spatial rotation-based correlation is greater than (for positive correlations) or less than (for negative correlations) the empirical correlation, divided by the number of spatial rotations. Here, we generated a null distribution based on 10,000 spatial rotations. Spin tests were implemented using the *rotate_parcellation* algorithm in R (https://github.com/frantisekvasa/rotate_parcellation)[88].

Supplementary Material

Refer to Web version on PubMed Central for supplementary material.

ACKNOWLEDGEMENTS

This study was supported by grants from the National Institute of Health: R01MH113550 to TDS and DSB, R01MH120482 to TDS, R01MH112847 to RTS and TDS, R01MH119219 to RCG and REG, R01MH123563 to RTS, R01MH119185 to DRR, R01MH120174 to DRR, R01NS060910 to RTS, R01EB022573 to TDS, RF1MH116920 to TDS and DSB, RF1MH121867 to TDS, R37MH125829 to TDS, R34DA050297 to APM, K08MH120564 to AAB, K99MH127293 to BL, and T32MH014654 to JS. VJS was supported by a National Science Foundation Graduate Research Fellowship (DGE-1845298). The Philadelphia Neurodevelopmental Cohort was supported by RC2 grants MH089983 and MH089924. Additional support was provided by the Penn-CHOP Lifespan Brain Institute.

DATA AVAILABILITY

The current study analyzes an existing, publicly available dataset from the Philadelphia Neurodevelopmental Cohort, available in the Database of Genotypes and Phenotypes (phs000607.v3.p2) at https://www.ncbi.nlm.nih.gov/projects/gap/cgi-bin/study.cgi?study_id=phs000607.v3.p2. Study analyses additionally made use of publicly available cortical atlases including the HCP multimodal atlas (downloaded from https://github.com/PennLINC/xcp_d/blob/main/xcp_d/data/ciftiatlas/glasser_space-fsLR_den-32k_desc-atlas.dlabel.nii), the Schaefer-400 atlas (downloaded from https://github.com/PennLINC/xcp_d/blob/main/xcp_d/data/ciftiatlas/Schaefer2018_400Parcels_17Networks_order.dlabel.nii), and the sensorimotor-association axis (downloaded from https://pennlinc.github.io/S-A_ArchetypalAxis/). Data derivatives from the current study, including development effect and environment effect maps, are available for download from https://doi.org/10.5281/zenodo.7606653.

REFERENCES

1. Sydnor VJ & Satterthwaite TD Neuroimaging of plasticity mechanisms in the human brain: from critical periods to psychiatric conditions. Neuropsychopharmacology 48, 219–220 (2023). [PubMed: 35963892]
2. Cooper EA & Mackey AP Sensory and cognitive plasticity: implications for academic interventions. Curr. Opin. Behav. Sci. 10, 21–27 (2016). [PubMed: 27231716]
3. Sisk LM & Gee DG Stress and adolescence: vulnerability and opportunity during a sensitive window of development. Curr. Opin. Psychol. 44, 286–292 (2022). [PubMed: 34818623]
4. Sydnor VJ et al. Neurodevelopment of the association cortices: Patterns, mechanisms, and implications for psychopathology. Neuron 109, 2820–2846 (2021). [PubMed: 34270921]
5. Bethlehem RAI et al. Brain charts for the human lifespan. Nature 604, 525–533 (2022). [PubMed: 35388223]
6. Gogtay N et al. Dynamic mapping of human cortical development during childhood through early adulthood. Proc. Natl. Acad. Sci. USA 101, 8174–8179 (2004). [PubMed: 15148381]
7. Dong H-M, Margulies DS, Zuo X-N & Holmes AJ Shifting gradients of macroscale cortical organization mark the transition from childhood to adolescence. Proc. Natl. Acad. Sci. USA 118, e2024448118 (2021). [PubMed: 34260385]
8. Grydeland H et al. Waves of Maturation and Senescence in Micro-structural MRI Markers of Human Cortical Myelination over the Lifespan. Cereb. Cortex 29, 1369–1381 (2019). [PubMed: 30590439]
9. Paquola C et al. Shifts in myeloarchitecture characterise adolescent development of cortical gradients. Elife 8, e50482 (2019). [PubMed: 31724948]
10. Huttenlocher PR & Dabholkar AS Regional differences in synaptogenesis in human cerebral cortex. J. Comp. Neurol. 387, 167–178 (1997). [PubMed: 9336221]
11. Larsen B & Luna B Adolescence as a neurobiological critical period for the development of higher-order cognition. Neurosci. Biobehav. Rev. 94, 179–195 (2018). [PubMed: 30201220]
12. García-Cabezas MÁ, Zikopoulos B & Barbas H The Structural Model: a theory linking connections, plasticity, pathology, development and evolution of the cerebral cortex. Brain Struct. Funct. 224, 985–1008 (2019). [PubMed: 30739157]
13. Huntenburg JM, Bazin P-L & Margulies DS Large-Scale Gradients in Human Cortical Organization. Trends Cogn. Sci. 22, 21–31 (2018). [PubMed: 29203085]
14. Margulies DS et al. Situating the default-mode network along a principal gradient of macroscale cortical organization. Proc. Natl. Acad. Sci. USA 113, 12574–12579 (2016). [PubMed: 27791099]
15. Hilgetag CC, Goulas A & Changeux J-P A natural cortical axis connecting the outside and inside of the human brain. Netw. Neurosci. 6, 950–959 (2022). [PubMed: 36875013]

16. Reh RK et al. Critical period regulation across multiple timescales. Proc. Natl Acad. Sci. USA 117, 23242–23251 (2020). [PubMed: 32503914]
17. Lensjø KK, Lepperød ME, Dick G, Hafting T & Fyhn M Removal of Perineuronal Nets Unlocks Juvenile Plasticity Through Network Mechanisms of Decreased Inhibition and Increased Gamma Activity. J. Neurosci. 37, 1269–1283 (2017). [PubMed: 28039374]
18. Martini FJ, Guillamón-Vivancos T, Moreno-Juan V, Valdeolmillos M & López-Bendito G Spontaneous Activity in Developing Thalamic and Cortical Sensory Networks. Neuron 109, 2519–2534 (2021). [PubMed: 34293296]
19. Frye CG & MacLean JN Spontaneous activations follow a common developmental course across primary sensory areas in mouse neocortex. J. Neurophysiol. 116, 431–437 (2016). [PubMed: 27146981]
20. Golshani P et al. Internally mediated developmental desynchronization of neocortical network activity. J. Neurosci. 29, 10890–10899 (2009). [PubMed: 19726647]
21. Nakazawa S, Yoshimura Y, Takagi M, Mizuno H & Iwasato T Developmental Phase Transitions in Spatial Organization of Spontaneous Activity in Postnatal Barrel Cortex Layer 4. J. Neurosci. 40, 7637–7650 (2020). [PubMed: 32887743]
22. Toyoizumi T et al. A theory of the transition to critical period plasticity: inhibition selectively suppresses spontaneous activity. Neuron 80, 51–63 (2013). [PubMed: 24094102]
23. Chini M, Pfeffer T & Hanganu-Opatz I An increase of inhibition drives the developmental decorrelation of neural activity. eLife 11, e78811 (2022). [PubMed: 35975980]
24. Fagiolini M & Hensch TK Inhibitory threshold for critical-period activation in primary visual cortex. Nature 404, 183–186 (2000). [PubMed: 10724170]
25. McGee AW, Yang Y, Fischer QS, Daw NW & Strittmatter SM Experience-Driven Plasticity of Visual Cortex Limited by Myelin and Nogo Receptor. Science 309, 2222–2226 (2005). [PubMed: 16195464]
26. Laumann TO & Snyder AZ Brain activity is not only for thinking. Curr. Opin. Behav. Sci. 40, 130–136 (2021).
27. Luhmann HJ et al. Spontaneous Neuronal Activity in Developing Neocortical Networks: From Single Cells to Large-Scale Interactions. Front. Neural Circuits 10, 40 (2016). [PubMed: 27252626]
28. Lake EMR et al. Simultaneous cortex-wide fluorescence Ca2+ imaging and whole-brain fMRI. Nat. Methods 17, 1262–1271 (2020). [PubMed: 33139894]
29. Ma Z, Zhang Q, Tu W & Zhang N Gaining insight into the neural basis of resting-state fMRI signal. NeuroImage 250, 118960 (2022). [PubMed: 35121182]
30. Magri C, Schridde U, Murayama Y, Panzeri S & Logothetis NK The Amplitude and Timing of the BOLD Signal Reflects the Relationship between Local Field Potential Power at Different Frequencies. J. Neurosci. 32, 1395–1407 (2012). [PubMed: 22279224]
31. Shmuel A & Leopold DA Neuronal correlates of spontaneous fluctuations in fMRI signals in monkey visual cortex: Implications for functional connectivity at rest. Hum. Brain Mapp. 29, 751–761 (2008). [PubMed: 18465799]
32. Yu-Feng Z et al. Altered baseline brain activity in children with ADHD revealed by resting-state functional MRI. Brain Dev. 29, 83–91 (2007). [PubMed: 16919409]
33. Fair DA & Yeo BTT Precision Neuroimaging Opens a New Chapter of Neuroplasticity Experimentation. Neuron 107, 401–403 (2020). [PubMed: 32758445]
34. Markicevic M et al. Cortical Excitation:Inhibition Imbalance Causes Abnormal Brain Network Dynamics as Observed in Neurodevelopmental Disorders. Cereb. Cortex 30, 4922–4937 (2020). [PubMed: 32313923]
35. Newbold DJ et al. Plasticity and Spontaneous Activity Pulses in Disused Human Brain Circuits. Neuron 107, 580–589.e6 (2020). [PubMed: 32778224]
36. Hinton EA, Li DC, Allen AG & Gourley SL Social Isolation in Adolescence Disrupts Cortical Development and Goal-Dependent Decision-Making in Adulthood, Despite Social Reintegration. eNeuro 6, ENEURO.0318–19.2019 (2019).

37. Greifzu F et al. Environmental enrichment extends ocular dominance plasticity into adulthood and protects from stroke-induced impairments of plasticity. Proc. Natl. Acad. Sci. USA 111, 1150–1155 (2014). [PubMed: 24395770]
38. Favuzzi E et al. Activity-Dependent Gating of Parvalbumin Interneuron Function by the Perineuronal Net Protein Brevican. Neuron 95, 639–655.e10 (2017). [PubMed: 28712654]
39. Tooley UA, Bassett DS & Mackey AP Environmental influences on the pace of brain development. Nat. Rev. Neurosci. 22, 372–384 (2021). [PubMed: 33911229]
40. Colich NL, Rosen ML, Williams ES & McLaughlin KA Biological Aging in Childhood and Adolescence Following Experiences of Threat and Deprivation: A Systematic Review and Meta-Analysis. Psychol. Bull 146, 721–764 (2020). [PubMed: 32744840]
41. McDermott CL et al. Early life stress is associated with earlier emergence of permanent molars. Proc. Natl. Acad. Sci. USA 118, e2105304118 (2021). [PubMed: 34103399]
42. Baum GL et al. Graded Variation in T1w/T2w Ratio during Adolescence: Measurement, Caveats, and Implications for Development of Cortical Myelin. J. Neurosci. 42, 5681–5694 (2022). [PubMed: 35705486]
43. de Faria O et al. Periods of synchronized myelin changes shape brain function and plasticity. Nat. Neurosci. 24, 1508–1521 (2021). [PubMed: 34711959]
44. Kato D et al. Motor learning requires myelination to reduce asynchrony and spontaneity in neural activity. Glia 68, 193–210 (2020). [PubMed: 31465122]
45. Burt JB et al. Hierarchy of transcriptomic specialization across human cortex captured by structural neuroimaging topography. Nat. Neurosci. 21, 1251–1259 (2018). [PubMed: 30082915]
46. Hill J et al. Similar patterns of cortical expansion during human development and evolution. Proc. Natl. Acad. Sci. USA 107, 13135–13140 (2010). [PubMed: 20624964]
47. Moore TM et al. Characterizing social environment's association with neurocognition using census and crime data linked to the Philadelphia Neurodevelopmental Cohort. Psychol. Med. 46, 599–610 (2016). [PubMed: 26492931]
48. Tooley UA et al. Associations between Neighborhood SES and Functional Brain Network Development. Cereb. Cortex 30, 1–19 (2020). [PubMed: 31220218]
49. O'Leary DDM, Chou S-J & Sahara S Area Patterning of the Mammalian Cortex. Neuron 56, 252–269 (2007). [PubMed: 17964244]
50. Charvet CJ & Finlay BL Evo-devo and the primate isocortex: the central organizing role of intrinsic gradients of neurogenesis. Brain Behav. Evol. 84, 81–92 (2014). [PubMed: 25247448]
51. Ackman JB, Burbridge TJ & Crair MC Retinal waves coordinate patterned activity throughout the developing visual system. Nature 490, 219–225 (2012). [PubMed: 23060192]
52. Benders MJ et al. Early Brain Activity Relates to Subsequent Brain Growth in Premature Infants. Cereb. Cortex 25, 3014–3024 (2015). [PubMed: 24867393]
53. Winnubst J, Cheyne JE, Niculescu D & Lohmann C Spontaneous Activity Drives Local Synaptic Plasticity In Vivo. Neuron 87, 399–410 (2015). [PubMed: 26182421]
54. Takesian AE & Hensch TK Chapter 1 - Balancing Plasticity/Stability Across Brain Development. in Progress in Brain Research (eds. Merzenich MM, Nahum M & Van Vleet TM) vol. 207 3–34 (Elsevier, 2013). [PubMed: 24309249]
55. Carulli D et al. Animals lacking link protein have attenuated perineuronal nets and persistent plasticity. Brain 133, 2331–2347 (2010). [PubMed: 20566484]
56. Anderson KM et al. Transcriptional and imaging-genetic association of cortical interneurons, brain function, and schizophrenia risk. Nat. Commun. 11, 2889 (2020). [PubMed: 32514083]
57. Micheva KD et al. A large fraction of neocortical myelin ensheathes axons of local inhibitory neurons. eLife 5, e15784 (2016). [PubMed: 27383052]
58. Condé F, Lund JS & Lewis DA The hierarchical development of monkey visual cortical regions as revealed by the maturation of parvalbumin-immunoreactive neurons. Brain Res. Dev. Brain Res. 96, 261–276 (1996). [PubMed: 8922688]
59. Benoit LJ et al. Adolescent thalamic inhibition leads to long-lasting impairments in prefrontal cortex function. Nat. Neurosci. 25, 714–725 (2022). [PubMed: 35590075]

60. Acevedo-Garcia D et al. Racial And Ethnic Inequities In Children's Neighborhoods: Evidence From The New Child Opportunity Index 2.0. Health Affairs 39, 1693–1701 (2020). [PubMed: 33017244]
61. Norbom LB et al. Parental socioeconomic status is linked to cortical microstructure and language abilities in children and adolescents. Dev. Cogn. Neurosci. 56, 101132 (2022). [PubMed: 35816931]
62. Piekarski DJ, Boivin JR & Wilbrecht L Ovarian hormones organize the maturation of inhibitory neurotransmission in the frontal cortex at puberty onset in female mice. Curr. Biol. 27, 1735–1745.e3 (2017). [PubMed: 28578932]
63. Kobayashi Y, Ye Z & Hensch TK Clock Genes Control Cortical Critical Period Timing. Neuron 86, 264–275 (2015). [PubMed: 25801703]
64. Konstantinides N et al. A complete temporal transcription factor series in the fly visual system. Nature 604, 316–322 (2022). [PubMed: 35388222]
65. Nielsen AN et al. Maturation of large-scale brain systems over the first month of life. Cereb. Cortex bhac242 (2022) doi:10.1093/cercor/bhac242.

METHODS-ONLY REFERENCES

66. Satterthwaite TD et al. Neuroimaging of the Philadelphia neurodevelopmental cohort. NeuroImage 86, 544–553 (2014). [PubMed: 23921101]
67. Esteban O et al. fMRIPrep: a robust preprocessing pipeline for functional MRI. Nat. Methods 16, 111–116 (2019). [PubMed: 30532080]
68. Avants BB et al. A reproducible evaluation of ANTs similarity metric performance in brain image registration. NeuroImage 54, 2033–2044 (2011). [PubMed: 20851191]
69. Dale AM, Fischl B & Sereno MI Cortical surface-based analysis. I. Segmentation and surface reconstruction. NeuroImage 9, 179–194 (1999). [PubMed: 9931268]
70. Ciric R et al. Benchmarking of participant-level confound regression strategies for the control of motion artifact in studies of functional connectivity. NeuroImage 154, 174–187 (2017). [PubMed: 28302591]
71. Ciric R et al. Mitigating head motion artifact in functional connectivity MRI. Nat. Protoc. 13, 2801–2826 (2018). [PubMed: 30446748]
72. Glasser MF et al. A multi-modal parcellation of human cerebral cortex. Nature 536, 171–178 (2016). [PubMed: 27437579]
73. Schaefer A et al. Local-Global Parcellation of the Human Cerebral Cortex from Intrinsic Functional Connectivity MRI. Cereb. Cortex 28, 3095–3114 (2018). [PubMed: 28981612]
74. Pham DD, Muschelli J & Mejia AF ciftiTools: A package for reading, writing, visualizing, and manipulating CIFTI files in R. NeuroImage 250, 118877 (2022). [PubMed: 35051581]
75. Cui Z et al. Individual Variation in Functional Topography of Association Networks in Youth. Neuron 106, 340–353.e8 (2020). [PubMed: 32078800]
76. Covitz S et al. Curation of BIDS (CuBIDS): A workflow and software package for streamlining reproducible curation of large BIDS datasets. NeuroImage 263, 119609 (2022). [PubMed: 36064140]
77. Wood SN Generalized Additive Models: An Introduction with R. (Chapman and Hall/CRC, 2017). doi:10.1201/9781315370279.
78. Simpson GL Modelling Palaeoecological Time Series Using Generalised Additive Models. Front. Ecol. Evol. 6, 149 (2018).
79. Satterthwaite TD et al. Impact of puberty on the evolution of cerebral perfusion during adolescence. Proc. Natl Acad. Sci. USA 111, 8643–8648 (2014). [PubMed: 24912164]
80. Reardon PK et al. Normative brain size variation and brain shape diversity in humans. Science 360, 1222–1227 (2018). [PubMed: 29853553]
81. Vaishnavi SN et al. Regional aerobic glycolysis in the human brain. Proc. Natl Acad. Sci. USA 107, 17757–17762 (2010). [PubMed: 20837536]

82. Yarkoni T, Poldrack RA, Nichols TE, Van Essen DC & Wager TD Large-scale automated synthesis of human functional neuroimaging data. Nat. Methods 8, 665–670 (2011). [PubMed: 21706013]

83. Paquola C et al. The BigBrainWarp toolbox for integration of BigBrain 3D histology with multimodal neuroimaging. eLife 10, e70119 (2021). [PubMed: 34431476]

84. Diedenhofen B & Musch J cocor: A Comprehensive Solution for the Statistical Comparison of Correlations. PLoS One 10, e0121945 (2015). [PubMed: 25835001]

85. Garrett DD, Lindenberger U, Hoge RD & Gauthier CJ Age differences in brain signal variability are robust to multiple vascular controls. Sci. Rep. 7, 10149 (2017). [PubMed: 28860455]

86. Adebimpe A et al. ASLPrep: a platform for processing of arterial spin labeled MRI and quantification of regional brain perfusion. Nat. Methods 19, 683–686 (2022). [PubMed: 35689029]

87. Alexander-Bloch AF et al. On testing for spatial correspondence between maps of human brain structure and function. NeuroImage 178, 540–551 (2018). [PubMed: 29860082]

88. Váša F et al. Adolescent Tuning of Association Cortex in Human Structural Brain Networks. Cereb. Cortex 28, 281–294 (2018). [PubMed: 29088339]

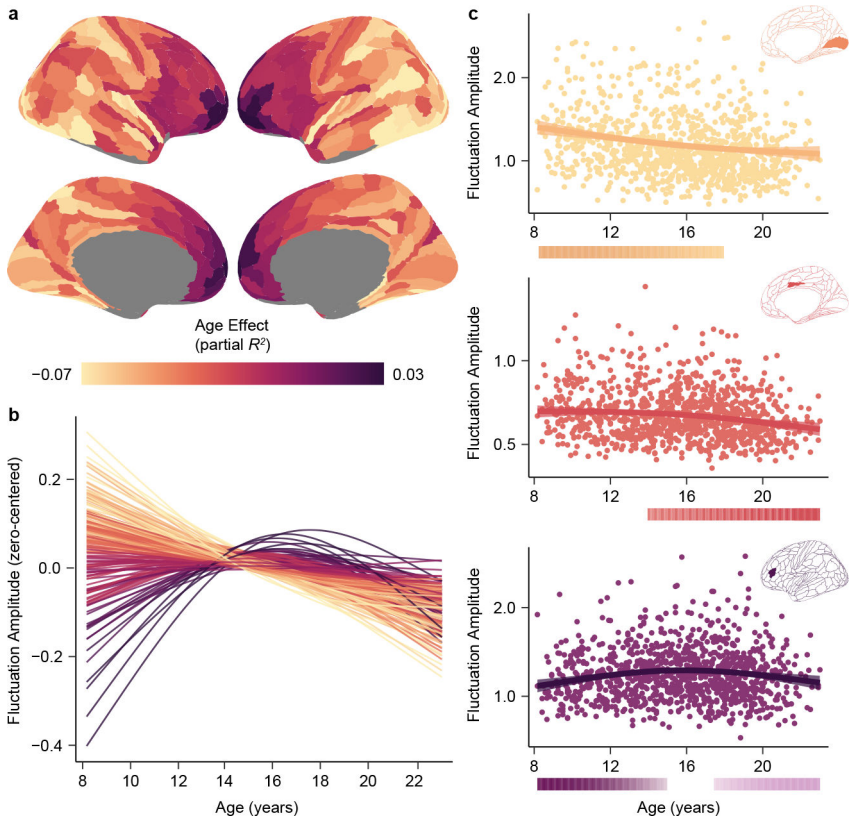

Fig. 1. Developmental refinement of fluctuation amplitude varies across the cortex.

a) The heterogeneous patterning of fluctuation amplitude age effects (partial R^2) is displayed across the cortical surface. **b)** Fluctuation amplitude developmental trajectories (zero-centered GAM smooth functions) are shown for all left hemisphere cortical regions, revealing a spectrum of age-related change. Trajectories are colored by each region's age effect using the color bar in panel a. **c**) Fluctuation amplitude developmental trajectories are shown overlaid on data from all participants for the primary visual cortex (area V1, yellow), the midcingulate gyrus (area p24pr, pink), and the dorsolateral prefrontal cortex (area IFSa, purple). Regional trajectories represent the GAM-predicted fluctuation amplitude value at each age with a 95% credible interval band. The color bars below each regional plot depict the age window(s) wherein fluctuation amplitude significantly changed in that region, shaded by the rate of change, as determined by the first derivative of the age function and the simultaneous 95% confidence interval around this derivative (two-sided).

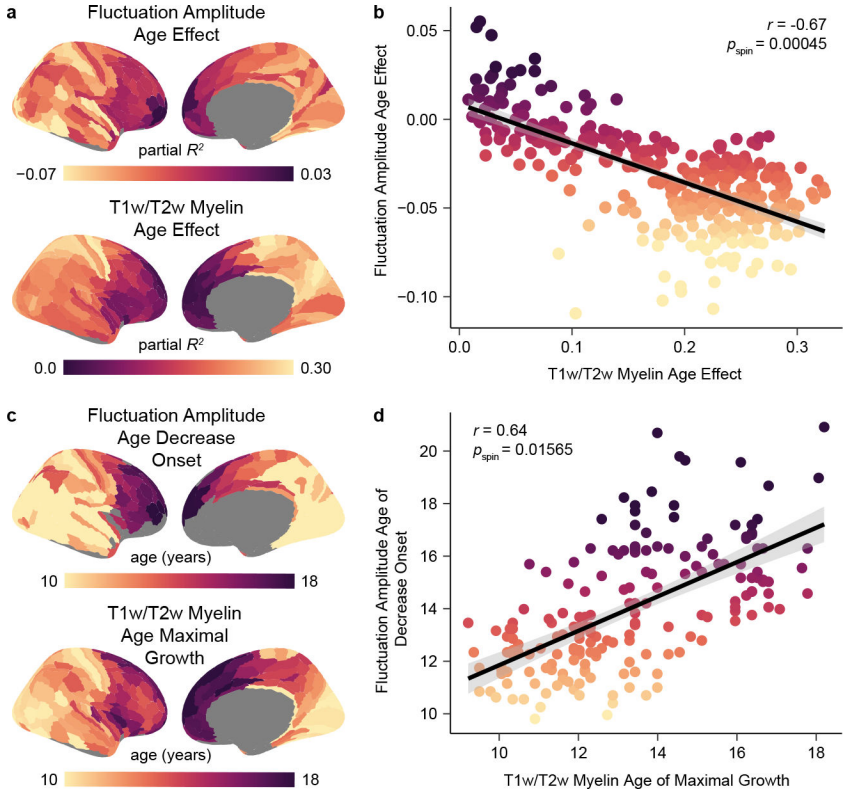

Fig. 2. Development of fluctuation amplitude spatially and temporally parallels cortical myelin development.

a) The cortical distribution of fluctuation amplitude age effects closely resembles the distribution of T1w/T2w ratio age effects, suggesting interdependent refinement of cortical function and microstructure in youth. Age effects (partial R^2) are signed by the sign of the average first derivative of the age smooth function. **b**) Regions that show larger declines in fluctuation amplitude during childhood and adolescence additionally undergo greater increases in the cortical T1w/T2w ratio in this developmental period. A Spearman's correlation between age effects for these two measures was significant ($r = -0.67$, $p_{spin} = 0.00045$) as assessed by a conservative spin-based spatial rotation test. The negative linear fit between these measures is shown with a 95% confidence interval. **c**) Maps depicting the age at which fluctuation amplitude began to decrease (earliest significant negative derivative of the age function) and the age of maximal T1w/T2w-indexed myelin growth (largest significant derivative of the age function) reveal temporal similarity in the development of these two measures in youth. **d**) Across regions, the age at which fluctuation amplitude began to significantly decrease is closely coupled to the age at which the T1w/T2w ratio shows a maximal rate of increase, providing evidence for temporal coordination between functional and structural maturation. A Spearman's correlation between these temporal measures was significant ($r = 0.64$, $p_{spin} = 0.01565$) as assessed by the spatial rotation test procedure. The positive linear relationship between these two measures is plotted with a 95% confidence interval.

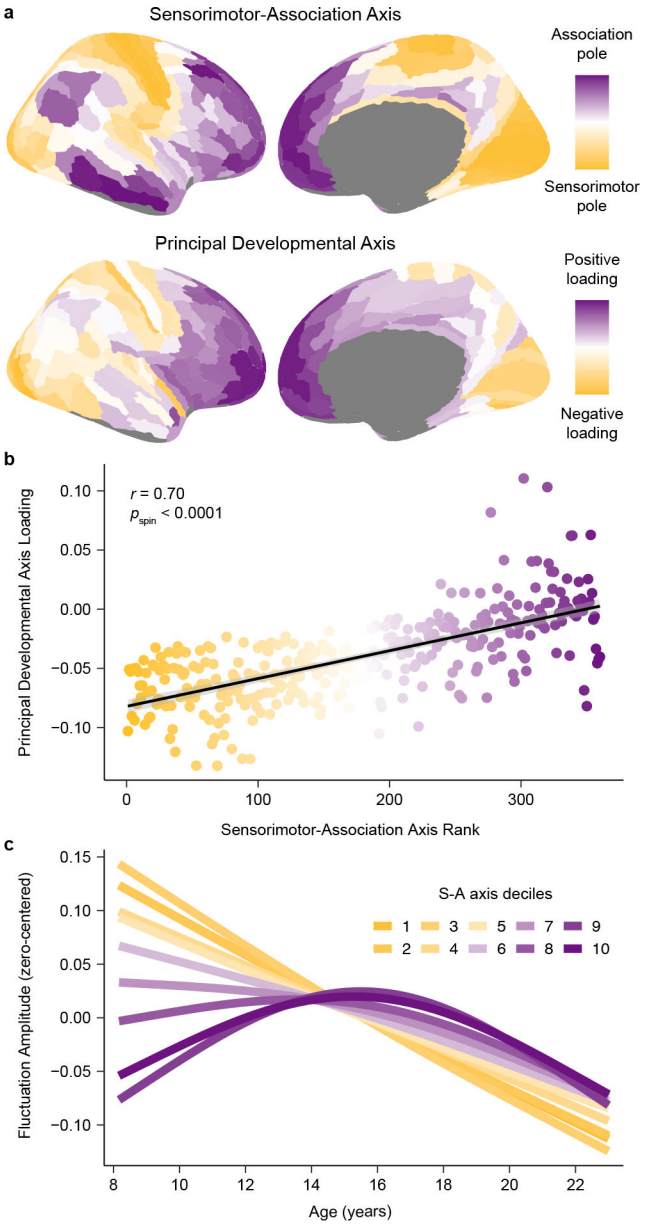

Fig. 3. The principal axis of fluctuation amplitude development exhibits convergent spatial embedding with the sensorimotor-association axis.

a) The principal axis of fluctuation amplitude development closely resembles the sensorimotor-association (S-A) axis, illustrating that the spatiotemporal maturation of intrinsic cortical fMRI activity aligns to the brain's global cortical hierarchy. The S-A axis, derived in Sydnor et al. (2021)[4], is a dominant axis of cortical feature organization that spans from primary sensory and motor cortices (sensorimotor pole; dark yellow), to modality-selective and multimodal cortices, and then to transmodal association cortices (association pole; dark purple). The principal developmental axis is the first component from a PCA conducted on regional fluctuation amplitude maturational trajectories. This component quantitatively captures cortex-wide differences in maturational patterns along a unidimensional spatial gradient. **b**) Across the cortex, principal developmental axis

loadings are strongly related to S-A axis ranks (linear association shown with a 95% confidence interval). The Spearman's correlation between these two measures, which represent developmental and organizational maps, was significant ($r = 0.70$, $p_{spin} < 0.0001$) as assessed by a conservative spin-based spatial rotation test. **c**) Average model fits depicting the relationship between fluctuation amplitude and age are shown for deciles of the S-A axis. To generate average decile fits, the S-A axis was divided into 10 bins each consisting of 33–34 regions, and age smooth functions were averaged across all regions in a bin. The first decile (darkest yellow; linear decline) represents the sensorimotor pole of the axis, the tenth (darkest purple; inverted U) represents the association pole of the axis. Maturational patterns diverged most between S-A axis poles and varied continuously between them.

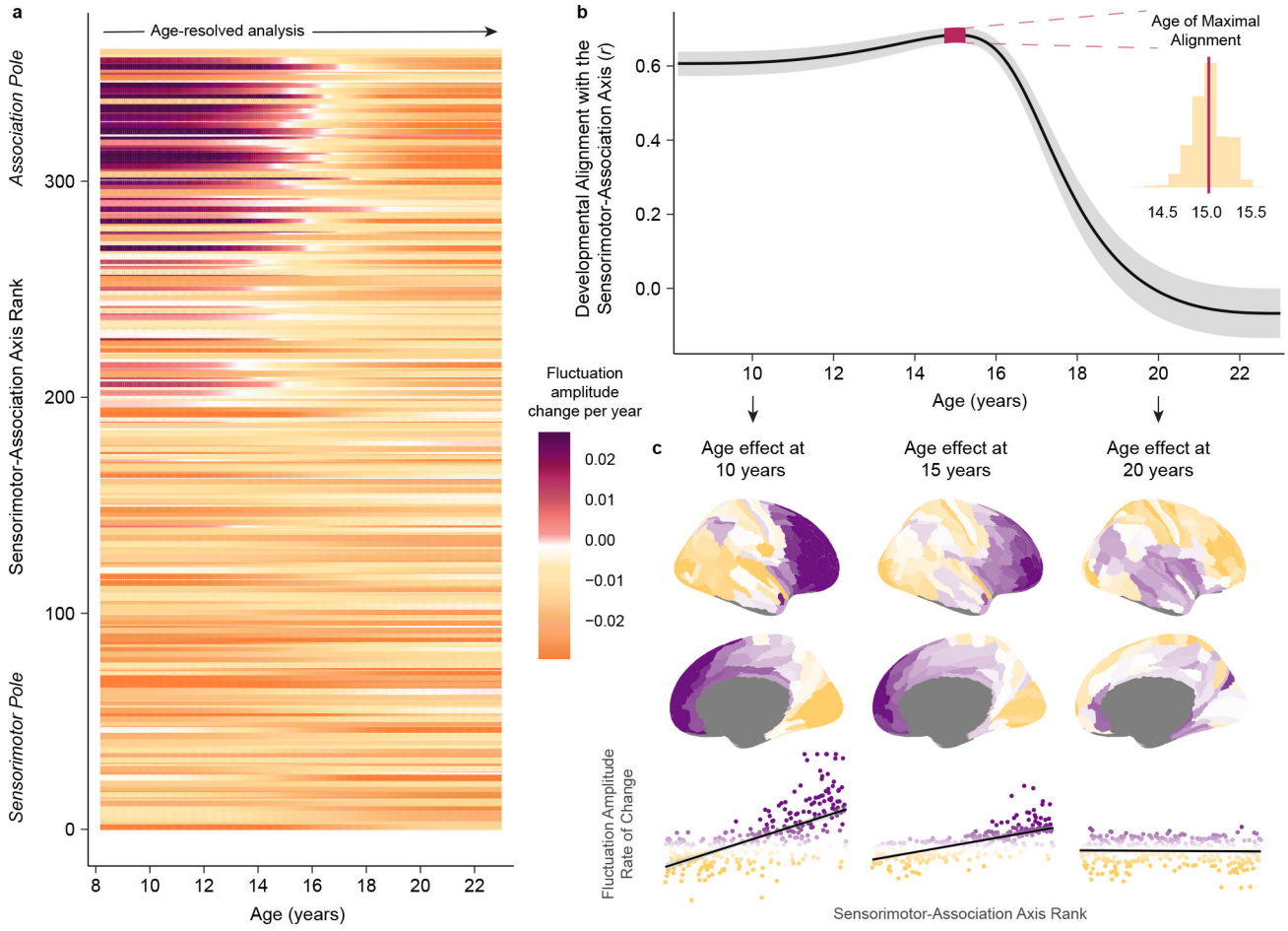

Fig. 4. Neurodevelopment unfolds along the sensorimotor-association axis until late adolescence.

a) The rate and direction of developmental change in fluctuation amplitude is displayed for each cortical region from ages 8 to 23 years. Regions are ordered along the y-axis by S-A axis rank. Fluctuation amplitude rate of change, expressed as the change in amplitude per year, was estimated from the first derivative of each region's GAM smooth function for age. Cortical regions near the association pole of the S-A axis exhibit unique increases in fluctuation amplitude through childhood that culminate in adolescent BOLD amplitude peaks. **b**) Developmental change in intrinsic fMRI activity aligns with the S-A axis from childhood until late adolescence. The line plot displays age-specific correlation values (*r*) between regional rates of fluctuation amplitude change and regional S-A axis ranks from ages 8 to 23 years. To obtain reliable estimates of this correlation value at each age, we sampled 10,000 draws from the posterior derivative of each region's age smooth function and quantified age-specific correlations between derivatives and S-A axis ranks for each draw. The median correlation value obtained across all draws is depicted by the black line and the 95% credible interval around this value is represented by the gray band. We additionally determined the age of maximal alignment between fluctuation amplitude change and S-A axis rank for all 10,000 draws. The 95% credible interval for the age of maximal alignment is depicted on the line plot by the pink band. The full distribution of ages obtained from all draws is portrayed in the inset histogram. **c**) Age-specific developmental

effects (first derivative maps) are visualized on the cortical surface at age 10, 15, and 20 years. Maps are shown above scatterplots that depict the linear relationship (with a 95% confidence interval band) between regional S-A axis ranks and regional age-specific rates of fluctuation amplitude change. Scatterplot points are colored by age-specific rates of change. Developmental refinement of fluctuation amplitude is governed by the S-A axis at ages 10 and 15 years. By age 20, further refinement of fluctuation amplitude is unrelated to the S-A axis.

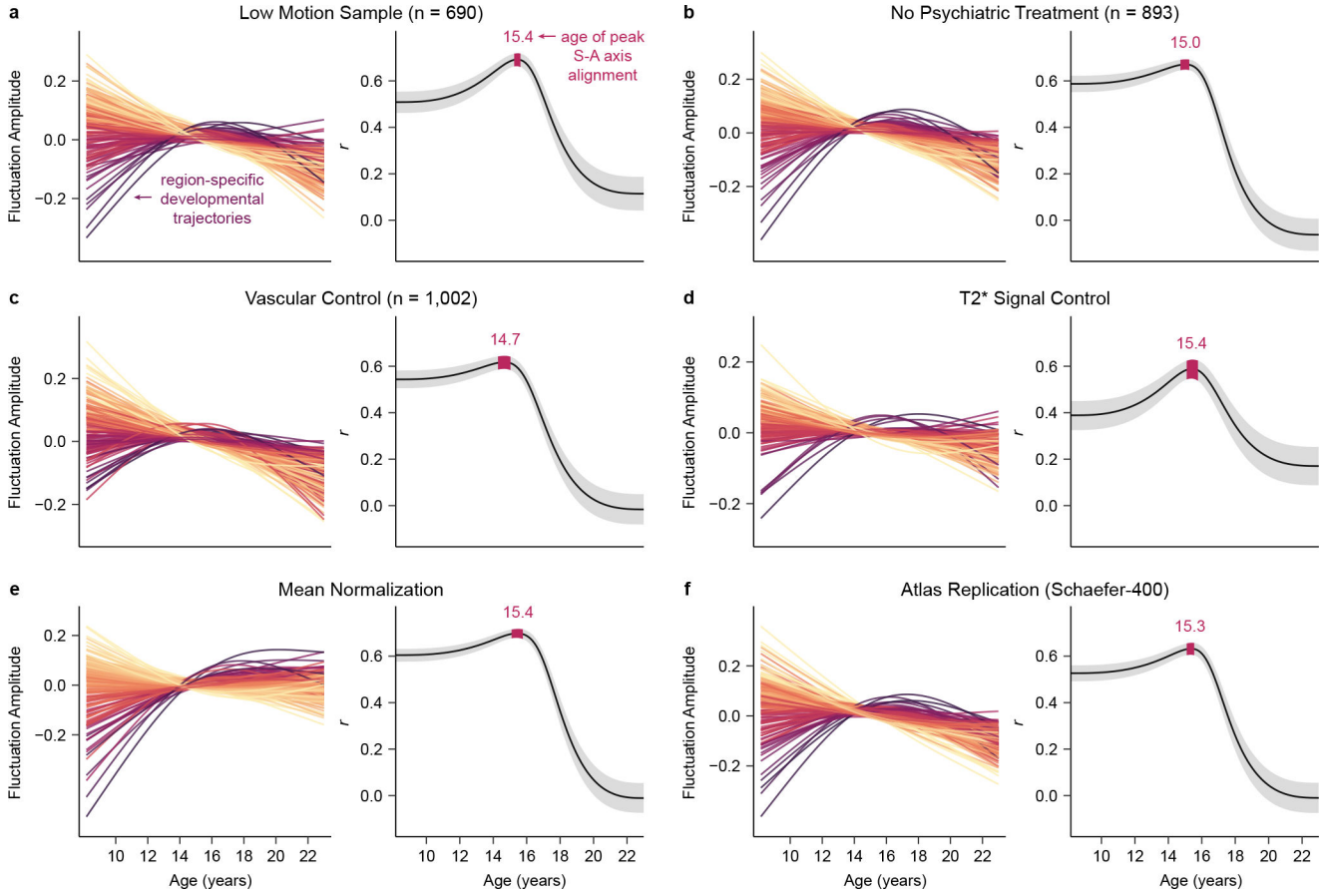

Fig. 5. Region-specific and cortex-wide developmental patterns are robust to methodological variation.

a-f) Key results are shown for each of the six sensitivity analyses performed. For each analysis, the left plot shows fluctuation amplitude developmental trajectories (zero-centered GAM smooth functions) for left hemisphere regions, colored by age effects. The right plot presents the age-resolved analysis of the correlation between developmental change in fluctuation amplitude and S-A axis rank from ages 8 to 23 years. Both the medial correlation value (*r*) and the 95% credible interval around this value are shown for the age-resolved analysis. All six sensitivity analyses yielded convergent region-specific and cortex-wide results, confirming that our developmental findings were not being driven by head motion in the scanner (a), the use of psychotropic medications (b), age-related changes in cerebrovascular perfusion (c), inter-scan differences in T2* signal strength (d), global effects (e), or the specific atlas used for cortical parcellation (f).

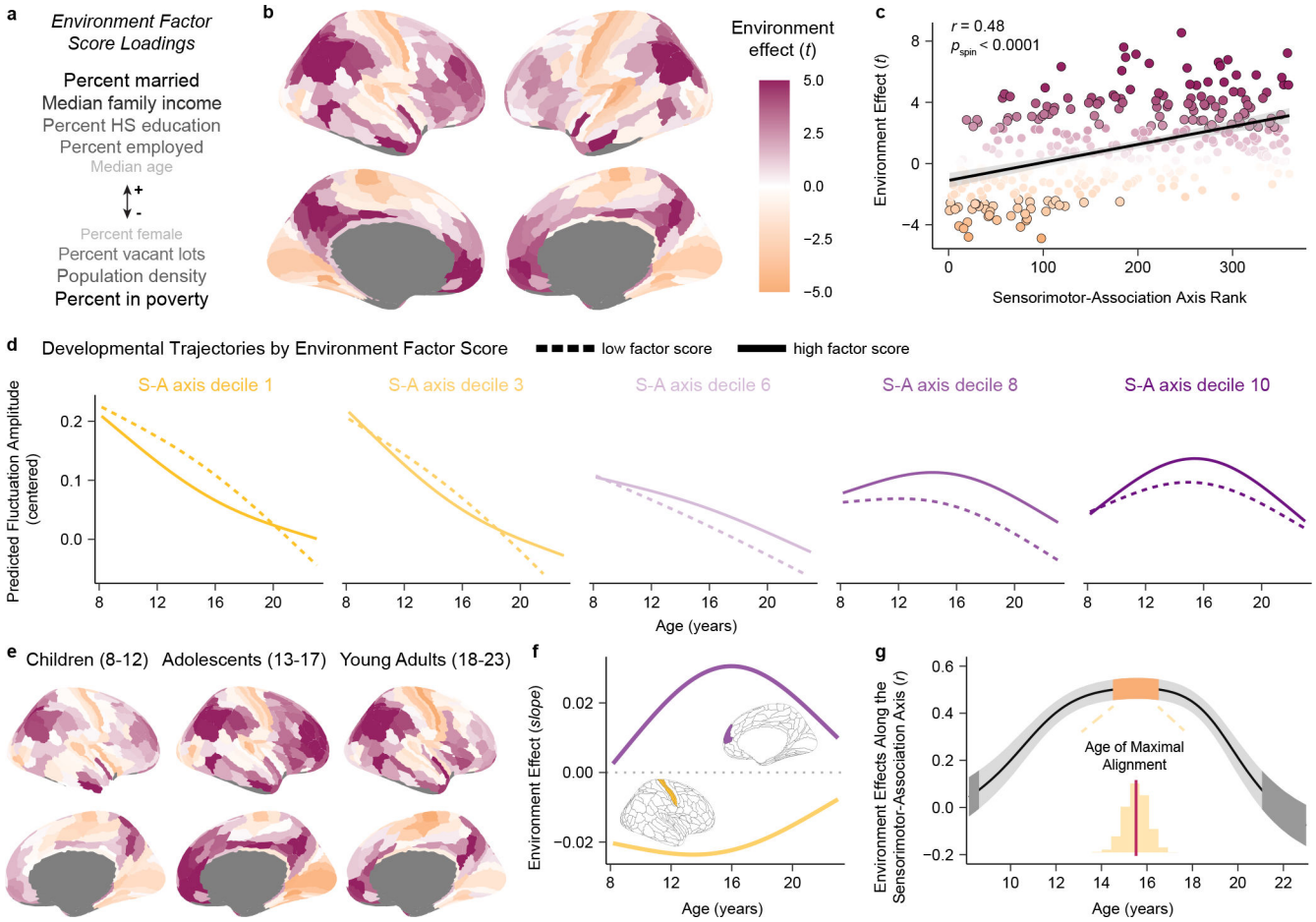

Fig. 6. Associations between fluctuation amplitude and the developmental environment vary along the sensorimotor-association axis in adolescence.

a) An environment factor score captures multiple features of each child's neighborhood environment. Variables listed above (+) and below (−) the arrow positively and negatively loaded onto the factor score, respectively. Darker and larger text indicates stronger loadings. Higher factor scores reflect greater neighborhood-level socioeconomic advantage. **b**) A cortical map displaying regional associations (quantified by model *t*-values) between environment factor scores and fluctuation amplitude is displayed; the map partly recapitulates the S-A axis. **c**) Each region's environment effect (*t*-value) is plotted against its S-A axis rank (linear fit shown with a 95% confidence interval). Regions with a significant environment effect following correction for multiple comparisons are outlined in black. The S-A axis explains significant variability in brain-environment associations (Spearman's correlation with a spatial rotation-based significance test: $r = 0.48$, $p_{spin} < 0.0001$). **d**) Fluctuation amplitude developmental trajectories are displayed for low and high environment factor scores for five deciles of the S-A axis, illustrating environment-associated differences in this measure by developmental timing. **e**) Cortical maps depicting region-wise associations between environment factor scores and fluctuation amplitude (as in b) in child, adolescent, and young adult groups show subtle differences in associations throughout development. Magenta and orange denote positive and negative environment effects (t-values), as in b. **f**) Age-specific environment effects are shown for an

exemplar primary sensorimotor region (primary somatosensory cortex, area 3b, yellow) and transmodal association region (medial prefrontal cortex, area 9m, purple). The magnitude of effects is largest in adolescence in these regions. **g**) Regional differences in environment associations are most organized along the S-A axis in adolescence, as revealed by age-specific correlations between regional environment effects and S-A axis ranks. The plot depicts the median correlation value (*r*) at each age (black line) and the 95% credible interval around this value (gray band) obtained by sampling the posterior distribution of regional age-by-environment interaction GAMs 10,000 times. The orange and dark gray bands respectively designate credible intervals for the ages of maximal and zero correlation of environment effects with the S-A axis.